ACSNANO

www.acsnano.org

REVIEW

Tailoring of Active Sites from Single to Dual Atom Sites for Highly Efficient Electrocatalysis

Hongwei Zhang, Xindie Jin, Jong-Min Lee,* and Xin Wang*

Cite This: *ACS Nano* 2022, 16, 17572–17592

Read Online

ACCESS | Metrics & More | Article Recommendations

ABSTRACT: Single atom catalysts (SACs) have been attracting extensive attention in electrocatalysis because of their unusual structure and extreme atom utilization, but the low metal loading and unified single site induced scaling relations may limit their activity and practical application. Tailoring of active sites at the atomic level is a sensible approach to break the existing limits in SACs. In this review, SACs were first discussed regarding carbon or non-carbon supports. Then, five tailoring strategies were elaborated toward improving the electrocatalytic activity of SACs, namely strain engineering, spin-state tuning engineering, axial functionalization engineering, ligand engineering, and porosity engineering, so as to optimize the electronic state of active sites, tune *d* orbitals of transition metals, adjust adsorption strength of intermediates, enhance electron transfer, and elevate mass transport efficiency. Afterward, from the angle of inducing electron redistribution and optimizing the adsorption nature of active centers, the synergistic effect from adjacent atoms and recent advances in tailoring strategies on active sites with binuclear configuration which include simple, homonuclear, and heteronuclear dual atom catalysts (DACs) were summarized. Finally, a summary and some perspectives for achieving efficient and sustainable electrocatalysis were presented based on tailoring strategies, design of active sites, and *in situ* characterization.

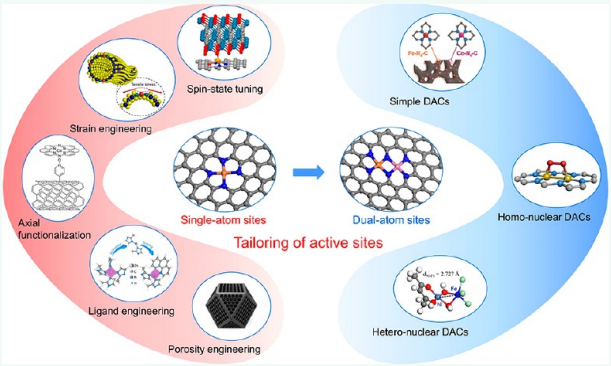

KEYWORDS: *Electrocatalysis, Single atom catalysts, Strain, Spin-state tuning, Axial functionalization, Ligand, Porosity, Dual atom catalysts*

INTRODUCTION

With the increasing concern for the environment and energy crisis, it is imperative to develop a clean and sustainable energy map.[1−3] Electrocatalysis has drawn intensive attention to many kinds of electrocatalytic conversions and chemical productions, such as the hydrogen evolution reaction (HER), oxygen evolution reaction (OER), oxygen reduction reaction (ORR), CO_2 reduction reaction (CO_2RR), and nitrogen reduction reaction (NRR).[4−9] The efficiency of electrocatalysis largely depends on the dynamics of these electrocatalytic reactions. Therefore, it is critical to design and construct a suitable electrocatalyst to alleviate the reaction energy barriers and elevate the reaction dynamics so as to achieve a highly efficient electrocatalysis energy path.[10−12] Generally, the transition metal electrocatalysts, especially noble metal nanoparticles, stand for a main category exhibiting excellent intrinsic activity.[13−15] Over the last decades, the high cost and scarce reserve of noble metals drive the development of the single atom catalysts (SACs), which is an ideal alternative to nanoparticles.[7,16−19] In addition to high atom utilization efficiency, SACs possess a well-defined structure for the catalytic site which is easy to use for model simulation and mechanistic study. The uniform structure also allows high electrocatalytic activity and selectivity, as demonstrated in a wide range of electrocatalytic applications.[20−22] Isolated single atoms such as active sites unfold another research dimension and promote the development of electrocatalysis.

Although SACs bear various benefits from their unusual structure, they may suffer from some drawbacks.[23,24] In general, single atoms tend to aggregate during synthesis and reaction processes, and adopting low metal loading in final catalysts is a common strategy to avoid the aggregation in reported SACs. Nevertheless, a high catalyst loading is necessary to realize a high overall electrocatalytic performance, which can potentially lead

Received: July 11, 2022
Accepted: November 1, 2022
Published: November 4, 2022

https://doi.org/10.1021/acsnano.2c06827
ACS Nano 2022, 16, 17572−17592

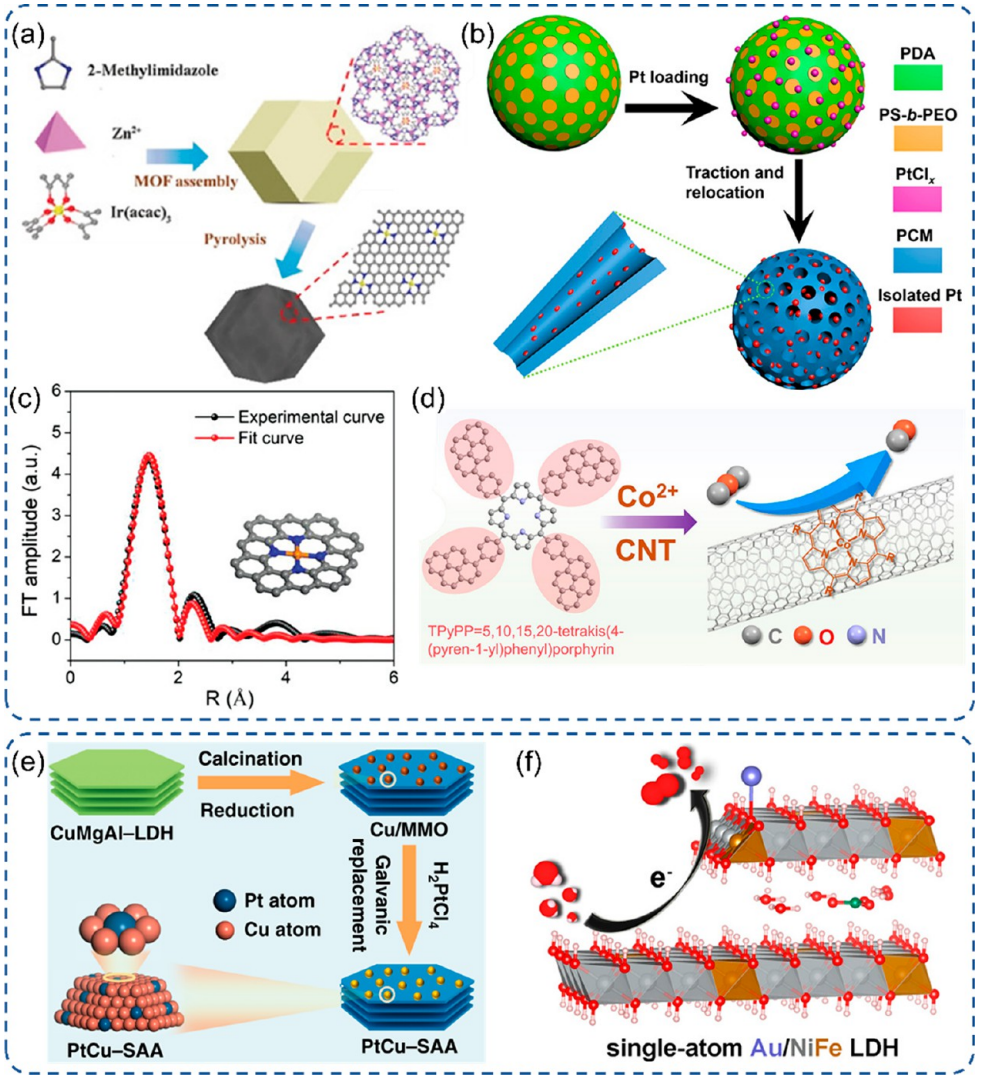

Figure 1. Schematic illustration of SAC synthesis on carbon or non-carbon supports. (a) Ir SACs based on MOF.[19] (b) Pt SACs based on a polymer.[48] (c) Fe SACs based on g-C_3N_4 with an EXAFS fitting curve.[53] (d) Co SACs based on CNTs.[50] (e) PtCu−SAA via a galvanic replacement reaction.[57] (f) Au/NiFe LDH SACs via the electrodeposition method.[63] (a) Reproduced with permission from ref 19. Copyright 2019 Wiley-VCH. (b) Reprinted with permission from AAAS and distributed under a Creative Commons CC BY-NC 4.0 License from ref 48. Copyright 2018 the Authors, some rights reserved; exclusive licensee AAAS. (c) Reproduced with permission under a Creative Commons CC BY License from ref 53. Copyright 2020 the Authors. (d) Reproduced with permission from ref 50. Copyright 2021 Wiley-VCH. (e) Reproduced with permission under a Creative Commons CC BY License from ref 57. Copyright 2019 the Authors. (f) Reproduced with permission from ref 63. Copyright 2018 American Chemical Society.

to a mass-transport issue. Although there are recent reports about the increased metal loading above 5 wt % in SACs by adopting sophisticated methods in lab scale,[25−28] the low metal loading and unsatisfactory metal site density are still the main challenges, and this is a long way from industrial applications, especially for traditional approaches such as wet chemistry based, simple high temperature pyrolysis, and atomic layer deposition.[21,29−32] On the other hand, a strong bond between isolated single atoms and supports can also contribute to the stability of SACs, but this strong interaction may also affect the electronic states of single atoms. Such an interaction can induce an electron-donation from metal atoms to supports, which yields more oxidic single atoms and manifestly alters the intrinsic activity. Lastly, the catalytic reactions always involve multiple steps and various intermediates, but the linear scaling relationship among the adsorption energy of intermediates can be significant when there is only one well-defined single atom configuration as active sites.[33] For example, considering the various key intermediates in the CO_2RR, such as *COOH, *CHO, *COH, and CO*, it is a dilemma to produce CO requiring a strong interaction of intermediates but a low desorption energy of CO.

To overcome these drawbacks and maximize the efficiency of SACs in electrocatalysis, it is critical to adopt realistic strategies and precise control to rationally manipulate the physicochemical properties of SACs in order to achieve high metal site density, suitable *d*-band center of active atoms and optimal binding strength with intermediates, fast electron communication with supports, high mass diffusion capability, and positive synergistic effect with adjacent atoms. Including the tuning of active sites and engineering of geometric structure, various approaches have been proposed over the past decades to modify the SACs at the atomic level.[34−37] For instance, the induced strain can considerably affect the electronic structure of single atoms.[38]

https://doi.org/10.1021/acsnano.2c06827
ACS Nano 2022, 16, 17572−17592

Furthermore, the ligand engineering can be applied to adjust the chemical state of single atoms via an electron-donating or withdrawing design.[36,39] For the low metal loading of SACs, the dual atom catalysts (DACs) with a configuration of atomic pairs may be a suitable solution to increase the metal loading.[23] Meanwhile, the presence of adjacent metal atoms not only affects the electronic state of the original single atom but also provides neighbor active sites. Although some reviews have already summarized the progress of SACs, there is still a lack of a comprehensive understanding of structure reactivity relationships at atomic levels, and more efforts are needed toward reasonable design and precise regulation of active sites to overcome the drawbacks of SACs.[17,21,40,41]

This critical review will first feature SACs based on classifications of carbon and non-carbon supports, followed by the exploring of five tailoring strategies with regard to electronic and geometric configurations to overcome the limitations of SACs, namely strain engineering, spin-state tuning engineering, axial functionalization engineering, ligand engineering, and porosity engineering. The synergistic effect on active sites and realization of dual atom catalysts (DACs) by introducing another atom were also inspected with respect to three categories, simple, homo-, and heteronuclear DACs. Lastly, a brief summary was presented with specific focus on the development of SACs, various tailoring engineering, and the progress of DACs with pair atoms. The existing problems and a possible future direction are also suggested.

RECENT ADVANCES IN SINGLE ATOM ELECTROCATALYSTS

Since the report of Pt SACs a decade ago,[42] significant progress has been achieved to obtain various precious metal SACs with maximum atom efficiency and robust electrocatalytic activity, especially in the kinetic sluggish ORR and CO_2RR processes. The support is essential for SACs as it not only provides the matrix to immobilize single atoms but also tunes the electronic state of single atoms via the control of bonding and coordination.[20] Here, we discussed the SACs based on carbon or non-carbon supports (Figure 1). On the one hand, carbon-based materials have been widely applied as supports, such as carbon nanotubes (CNTs), graphitic carbon nitride (g-C_3N_4), metal−organic framework (MOF) derived carbon, and polymer derived carbon. This is due to their high surface area, high conductivity, strong interaction with single atoms to manipulate its electronic structure, and easy functionalization by O, N, S, and P atoms. On the other hand, non-carbon substrates have gained increasing attention because of the ample choices of diverse materials with adjustable physicochemical properties, flexible structures and compositions, and high tolerance in harsh conditions.[17]

DESIGN AND SYNTHESIS OF SACS

Carbon-Based SACs. Based on the self-assembled coordination of metal nodes and ligands, together with tunable ligand type and tailorable morphology, MOF derived SACs demonstrated a great potential toward excellent electrocatalytic applications.[21,43] Yin et al. reported a facile pyrolysis of bimetallic Zn−Co zeolitic imidazolate frameworks (ZIF-8) with up to 4 wt % Co loading, which endows superior ORR activity and outstanding stability for at least 5000 continuous potential cycles.[44] By an encapsulation approach in MOFs, Xiao et al. synthesized the Ir−N−C SACs with ZIF-8 (cage and pore size diameters of 11.6 and 3.4 Å) as a host and encapsulated the Ir acetylacetonate molecule (diameter of 9.7 Å) as a guest (Figure 1a).[19] The Ir−N−C SACs displayed an excellent ORR performance and durability with no obvious decay after 5000 cycles. In order to improve the mass transport and expose more active sites, a two-dimensional MOF was exfoliated from bulk pillared-layer MOFs, showing efficient OER activity.[43] The pillar removal and exfoliation were based on an induced bent bridging angle and the lower strength of coordination bonds than covalent bonds.[45] Containing abundant heteroatoms as coordination centers, the polymer can also serve as the carbon precursor.[40] For example, a precursor-dilution method was proposed by He et al. to synthesize various M_1/N−C SACs up to 24 types (M = Mn, Co, Cu, Ru, Pd, Ag, and so on).[46] The tetraphenylporphyrin (TPP) chelated with metal cations, together with the parent TPP as the diluter to be copolymerized via Friedel−Crafts alkylation to form SACs with sufficient distance avoiding aggregation. Han and co-workers reported a polymer encapsulation strategy with only using dopamine to generate SACs showing nanosphere morphology.[47] The obtained Co SACs showed great durability with a slight decay after 5000 continuous cycles in the ORR. Including dopamine, Lou et al. added polystyrene-*block*-poly(ethylene oxide) (PS-*b*-PEO) as a sacrificial agent to form a porous nanosphere (Pt@PCM) with isolated Pt single atoms (Figure 1b).[48] The stability of Pt SACs was measured with no deactivation within 5 h during the *I-t* test in both acidic and alkaline conditions. Besides MOFs and polymers, CNTs, g-C_3N_4, and defective graphene are also reported as carbon substrates. Through the $\pi-\pi$ interaction (Figure 1d), the macrocyclic ligands chelated with metal sites can anchor on CNTs and graphene as single atom sites for the electrocatalytic reaction, such as the 1,10-phenanthroline-Cu complex.[49,50] In order to enhance the delocalized π electron orbital and $\pi-\pi$ interaction, Sun et al. adopted a planar configurated 4-macrocyclic ligand on CNTs endowing a great CO_2RR performance.[51] Parallel to the stronger $\pi-\pi$ interaction with CNTs, the enlarged π-conjugation of the ligand can further perturb the electron state of metal sites and boost the CO_2RR.[50] The single atom isolated on C_3N_4 can be synthesized via the simple mixing of porous C_3N_4 and metal precursors, followed by $NaBH_4$ reduction or the pyrolysis process (Figure 1c).[52,53] This can be attributed to the strong coordination properties of N sites with metal ions and a confined environment to repress the meal agglomeration. The synthesized FeN_4 SACs displayed good stability with an acceptable attenuation during a 24-h test. Using the atomic layer deposition (ALD) technique, Co SACs with 1 wt % loading can be successfully synthesized on the g-C_3N_4 substrate with bis(cyclopentadienyl)cobalt as the Co precursor and the unsaturated N atoms as metal anchor sites.[54] During the ALD process, a short O_3 treatment at 150 °C was necessary to remove surface ligands. The HAADF-STEM and XANES characterizations confirmed the isolated Co atoms and CoN_4 configurations. Meanwhile, Pd SACs loaded on the graphene support with 0.25 wt % loading can also be synthesized via the ALD approach after one cycle with palladium hexafluoroacetylacetate as the Pd precursor and surface phenolic oxygen species on graphene as metal anchor sites.[55] Over a thermal emitting method, the defective graphene substrate was based to generate Pt SACs exhibiting superior electrocatalytic activity.[56] During the thermal process, the dicyandiamide was first decomposed to release NH_3, followed by the formation of volatile $Pt(NH_3)_x$ via strong interaction of NH_3 and Pt net. The defects can be created by removing oxygen groups on graphene oxide, which can

https://doi.org/10.1021/acsnano.2c06827
ACS Nano 2022, 16, 17572−17592

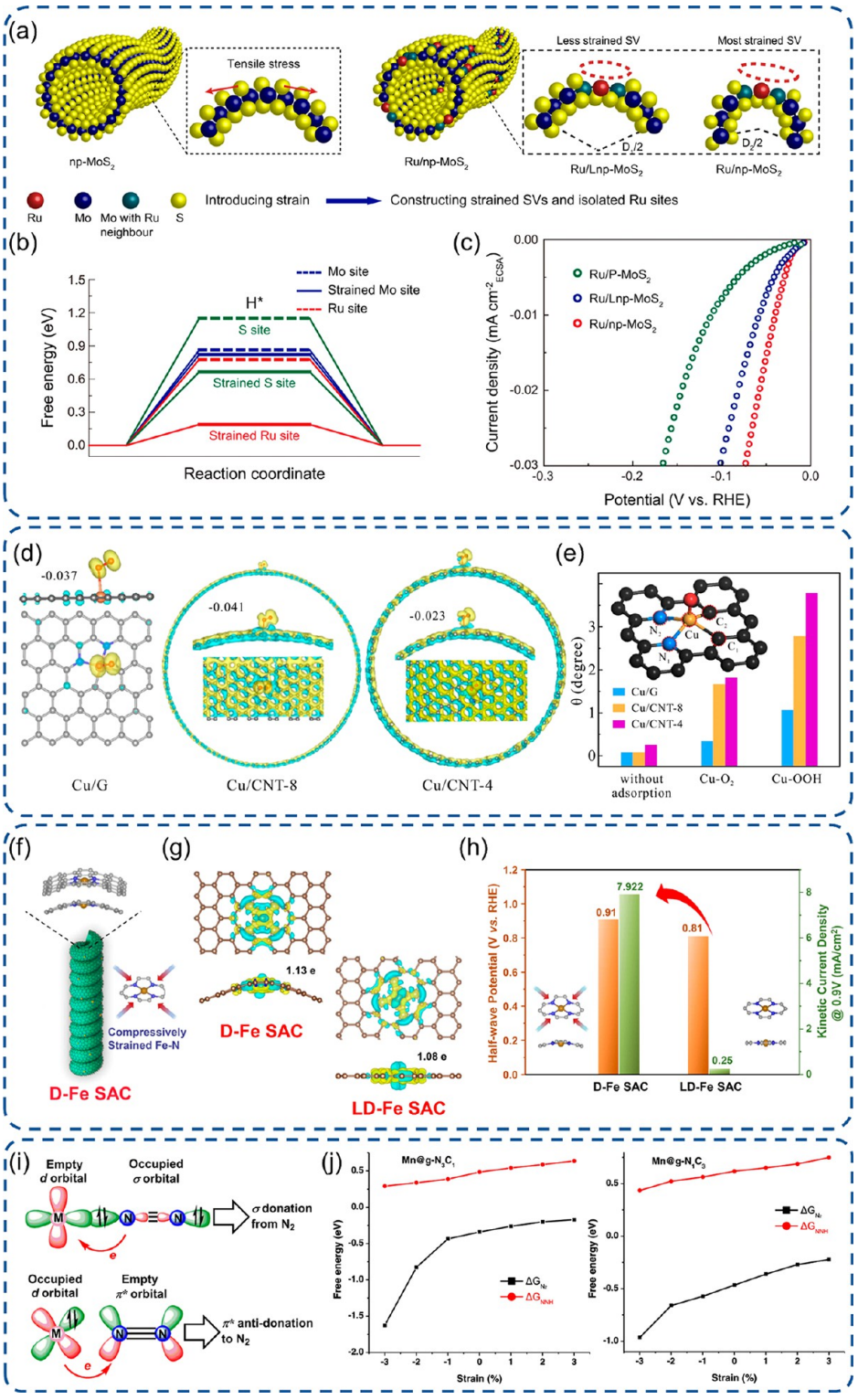

Figure 2. Engineering of SACs with tensile surface strain or compressive strain. (a) Schematic illustration of Ru SAC construction with tensile stress, (b) free energy profiles for hydrogen adsorption, and (c) ECSA-normalized polarization curves for Ru SACs.[73] (d) Side view and top view of the charge density difference of Cu SACs with different strains and (e) structure distortion of Cu sites at various stages of the ORR.[77] (f) Schematic illustration of D-Fe SAC with compressive strains, (g) charge density difference diagrams of Fe SACs with electron accumulation or depletion highlighted by yellow or cyan, and (h) half-wave potentials and kinetic current densities (0.9 V vs RHE) of Fe SACs in 0.1 M KOH.[81] (i) Schematic illustration of the fixation and activation of N_2 on active sites with two models and (j) simulated ΔG with varying extra strain from −3 to 3% on Mn SACs with g-N_3C_1 and g-N_1C_3 two configurations.[82] (a-c) Reproduced with permission under a Creative Commons CC BY License from ref 73. Copyright 2021 the Authors. (d-e) Reproduced with permission under a Creative Commons CC BY License from ref 77. Copyright 2021 the Authors. (f-h) Reproduced with permission from ref 81. Copyright 2021 Wiley-VCH. (i-j) Reproduced with permission under a Creative Commons CC BY-NC-ND 4.0 License from ref 82. Copyright 2021 American Chemical Society.

https://doi.org/10.1021/acsnano.2c06827
ACS Nano 2022, 16, 17572−17592

capture volatile $Pt(NH_3)_x$ and finally form Pt SACs. The excellent durability was demonstrated for Pt SACs with negligible change after a 24-h chronoamperometry test in an acidic solution for the HER.

Non-Carbon-Based SACs. The alloying strategy is an efficient way to anchor isolated atoms via strong interaction with host metals to enhance the catalytic activity. Ru−Pd alloying SACs were reported via the wet chemical method, and Pt−Cu alloying SACs were synthesized via a galvanic replacement reaction (Figure 1e).[57,58] Due to the Lewis acidic properties of some metal oxides, such as Al_2O_3 and Cr_2O_3, they are also potential candidates as supports for SACs. Cu SACs were constructed on a Lewis acidic support owing to the strong interaction and tunable electronic states of active sites.[59] The unaffected structure of the ultrathin nanosheet was verified by HRTEM manifesting considerable durability. Owing to enormous vacancies in amorphous materials, they can act as supports or even electrocatalysts displaying superior activity in comparison to the one with the crystalline structure in electrocatalysis.[60] Recently, Zhang et al. reported a Ga SACS immobilized on amorphous TiO_2 nanofibers expressing excellent N_2RR performance and structure stability in combination with a "π back-donation" behavior of *d*-block metals for easy activation of N_2 and a nature of stronger adsorption of N_2 than H_2 for *p*-block metals. The abundant oxygen vacancies in amorphous TiO_2 acted as anchor sites for single Ga atoms.[61] Metal hydroxides, especially layered double hydroxides, can be a suitable support for SACs due to their distinctive electronic properties and layered structure.[62] Zhang et al. achieved a 6-fold enhancement for OER activity with the synthesis of Au SACs on the NiFe layered double hydroxide (LDH) (Figure 1f).[63] The Au/NiFe LDH expressed outstanding activity and durability for the OER with no decay after 2000 continuous cycles. Metal chalcogenides, carbides, nitrides, and phosphides are another large tank to gain substantial attention.[17] Cao et al. studied the Ru doping on 2D MoS_2 to form Ru SACs accompanying MoS_2 phase transition and vacancy formation.[18] Zhang et al. applied a tunable electrochemical deposition method to immobilize Pt metal on CoP-based nanorod arrays in neutral media to realize a large area and scalable synthesis.[64,65] The Pt SACs can maintain the optimized performance with four times higher mass activity than Pt/C in the HER for 24 h. Using this powerful electrochemical deposition method, Zeng et al. reported a successful synthesis of Ir SACs on $Co(OH)_2$ based on either cathodic or anodic deposition with $IrCl^{3+}$ cations or $Ir(OH)_6^{2-}$ anions as deposition species, respectively.[66] The metal loading can be varied by precursor concentration, scanning cycles, and scanning rate. The obtained SACs displayed excellent activity and long-term stability for water splitting with cathodically deposited Ir SACs for the HER and anodically deposited Ir SACs for the OER. Different activities of two Ir SACs may be derived from the different oxidation states and coordination of metal centers.

ELECTRONIC AND GEOMETRIC TAILORING ENGINEERING

Strain Engineering. The energy level of adsorbates or intermediates on the catalyst surface with respect to one another is correlated to the activity of catalysts.[67] The strain effect is a practicable strategy, which can be triggered by lattice mismatch, compressive strain, or tensile strain to change the bond length.[68] Its application has already been rationalized to optimize the electronic state of active sites and manipulate the adsorption nature to achieve a positive effect on electrocatalytic activity.[38] It was considered as a long-range effect with a penetrating length of a few atomic layers.[69] Generally, microstrain was commonly induced by the mismatch of lattice or other associated structure defects, and strain engineering can be implemented via core−shell structure design,[70] dealloying strategy,[71] or even mechanical loading.[72] Herein, two common strain engineering strategies on SACs were discussed as tensile surface strain or compressive strain, induced by curvature design or lattice mismatch (Figure 2).

Kang et al. carried out an experimental inspection and density functional theory (DFT) calculation of the strain effect on single-atom Ru isolated on a MoS_2 support with the precisely tailored tensile stress via a curvature design (Figure 2a).[73] After applying tensile surface strain, the water adsorption energy significantly dropped on both isolated Ru atoms and adjacent Mo sites, showing a greater overlap between metal 3*d* orbits and 2*p* orbitals of adsorbed oxygen. Therefore, it will be of benefit to the dissociation of H_2O, and the energy barriers of the Volmer step will be decreased. Furthermore, the free energy of hydrogen adsorption was obviously reduced, which can induce a more efficient H−H coupling and better HER performance with a much lower Tafel slope and lower overpotential at E_{10} (10 mA/cm^2) for the most strained Ru/MoS_2 compared to the counterparts with less and no strain (Figure 2b,c). This indicates that the intrinsic catalytic activity is highly related to the strain effect on the Ru electronic structure. The molecular level modification of the linker in MOFs can significantly affect its properties, and a tensile strain was reported in a two-dimensional MOF after partial substitution of terephthalic acid linkers by ferrocene carboxylic acid (FcCA).[74,75] With the coordination of FcCA to two adjacent Co moieties, the tensile strain was generated leading to a regulation of the Co spin state from a high state ($t_{2g}^5e_g^2$) to a medium state ($t_{2g}^6e_g^1$), which can strengthen the adsorption of OH* and facilitate the rate-determining step of the formation of OOH* in the OER. Recently, Luo et al. reported Rh SACs via an atomic galvanic replacement method, and the tensile strain was introduced by the formation of atomic-layer-thick Pt shells via a subsequently electrochemical dealloying treatment.[76] The synthesized tensile-strained Rh SACs expressed significantly enhanced activity and stability for the ethanol oxidation reaction (EOR). The characterization of the Rh chemical state and DFT calculation revealed that the enhancement was derived from the stronger adsorption of ethanol and intermediates, especially for the CH_3CHO intermediate with the avoidance of the poisoning of electrocatalysts. Furthermore, the optimized adsorption nature of active sites stemmed from the tensile strain induced electron transfer from the matrix to Rh atoms and regulation of the *d*-band center of metal atoms toward the Fermi level.

During the electrochemical reaction process, the active sites may experience a distinctive dynamic evolution in terms of the configuration and electronic state due to the new bond formation via coordination with reactants and intermediates, especially under a tensile-strained environment. With the help of operando X-ray absorption fine structure (XAFS) characterization and DFT simulation, Han et al. demonstrated that the tensile strain has a significant effect on geometry distortion of active sites and further on its intrinsic ORR activity for designed Cu SACs (Figure 2d).[77] The Cu SACs with a CuN_2C_2 configuration were synthesized on three carbon-based substrates with different curvatures and surface tensile: graphene (mild strain) and CNTs with 8 nm (medium strain) and 4 nm

https://doi.org/10.1021/acsnano.2c06827
ACS Nano 2022, 16, 17572−17592

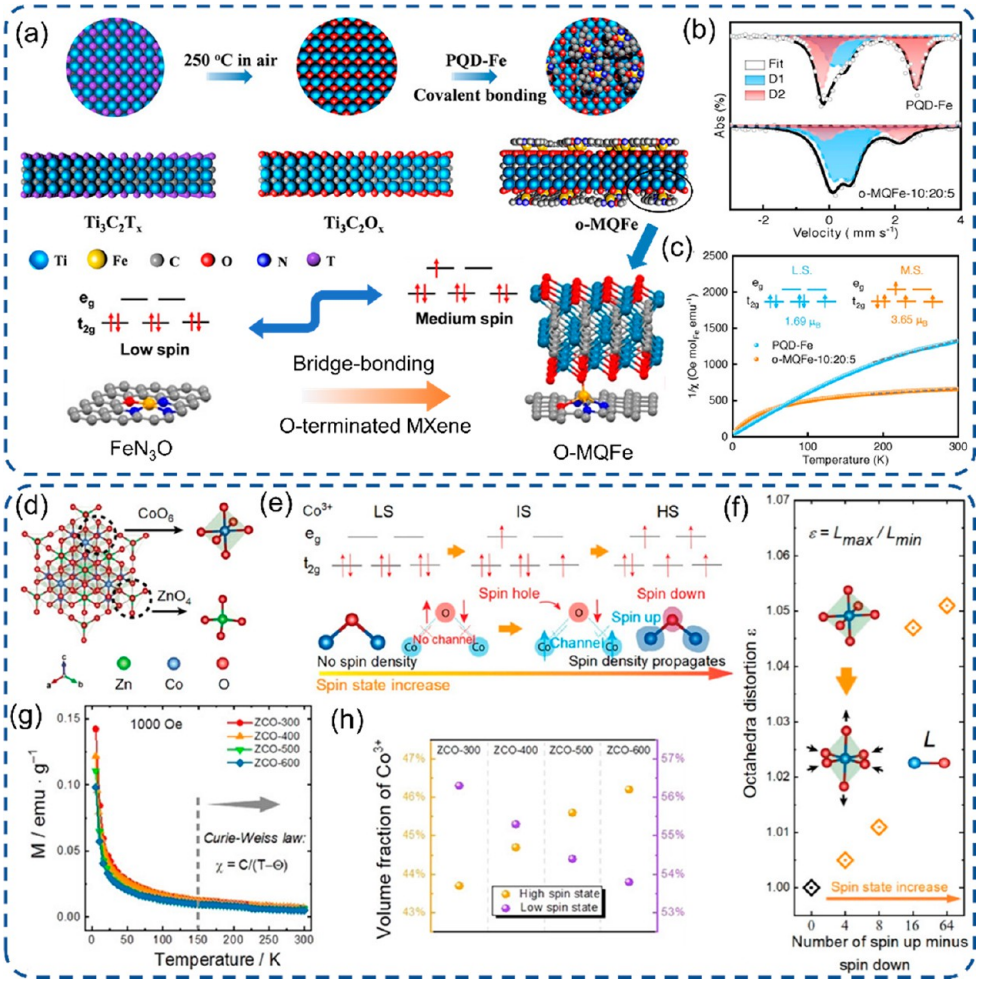

Figure 3. Engineering of SACs with the spin-state tuning strategy. (a) The synthesis process of Fe SACs and spin-state tuning of Fe^{III}, (b) ^{57}Fe Mössbauer spectroscopy with D1 and D2 peaks assigned to medium- and low-spin Fe^{III}, and (c) $1/\chi_m$ plots.[90] (d) Crystal structure of spinel $ZnCo_2O_4$ with Co in octahedral sites, (e) illustration of the Co^{3+} spin state and Co−O−Co spin channel with the rising of the cobalt spin state, (f) the octahedra distortion, (g) temperature-dependent magnetization characterizations of the as-prepared samples at H = 1000 Oe, and (h) the ratio of high and low spin state Co^{3+} calculated based on the effective magnetic moment.[92] (a-c) Reproduced with permission from ref 90. Copyright 2022 Wiley-VCH. (d-h) Reproduced with permission from ref 92. Copyright 2021 Wiley-VCH.

diameters (severe strain).[78] The high curvature induced strain in carbon frameworks is supposed to be released due to thermodynamic favor via structure distortion after the formation of new metal−adsorbate bonds. Both operando XAFS analysis and DFT calculation demonstrated this proof-of-concept. It pointed out that the boosted ORR activity was derived from the change of the chemical state of Cu and distortion probed by the elongated bond length and angle after the formation of the Cu−O bond with oxygenated species (Figure 2e); but the too mild distortion has no visible enhanced Cu−O electron transfer, whereas the too severe distortion will weaken the original CuN_2C_2 interaction and impair the electron transfer.

Fe centers in macrocyclic compounds always present too much of a strong adsorption nature, and the moderation of such strong binding with molecules can lift its ORR performance.[79,80] Adopting a self-assembled chiral surfactant, Jia et al. reported Fe SACs on a carbon-based support with a helical structure and high curvature induced compressive strain (Figure 2f,g).[81] The compressive strain was verified by the shortened Fe−N bond length from EXAFS results. The obtained compressive-strained Fe SACs granted a more positive onset potential from LSV curves, faster kinetics from Tafel slopes for the ORR in both alkaline and acidic electrolytes (Figure 2h), and higher power density in zinc-air battery devices. The enhanced intrinsic activity for the ORR is attributed to the weakened adsorption strength with oxygenated intermediates to Fe sites, which originated from the compressive strain causing larger Bader charge and a downshift of the *d*-band center for Fe sites. In the NRR process, the control of the adsorption nature and *d*-band center via strain engineering is also a meaningful strategy. From a theorical perspective, Li et al. simulated compressive and tensile strains by the creation of concave and convex regions via varying the lattice parameters within a range of −3 to 3% on 2D Mn SACs (Figure 2i,j).[82] The DFT simulation mainly focused on two critical steps: the adsorption of N_2 and first protonation of $*N_2$ to *NNH. It revealed that only an extra compressive strain can bring a decrease of the *d*-band center energy of Mn sites, which will boost NRR activity due to the rising of a stronger adsorption of N_2 and a decrease of Gibbs free energy changes for the first protonation process. For the Ru-based OER catalyst in acidic conditions, the sluggish activity and dissolution problem are the main challenges.[83] The issues are highly relevant to the metal redox state, the bonding strength of adsorbed oxygen, and oxygen diffusivity.[84] In order to obtain more insights and solve

https://doi.org/10.1021/acsnano.2c06827
ACS Nano 2022, 16, 17572−17592

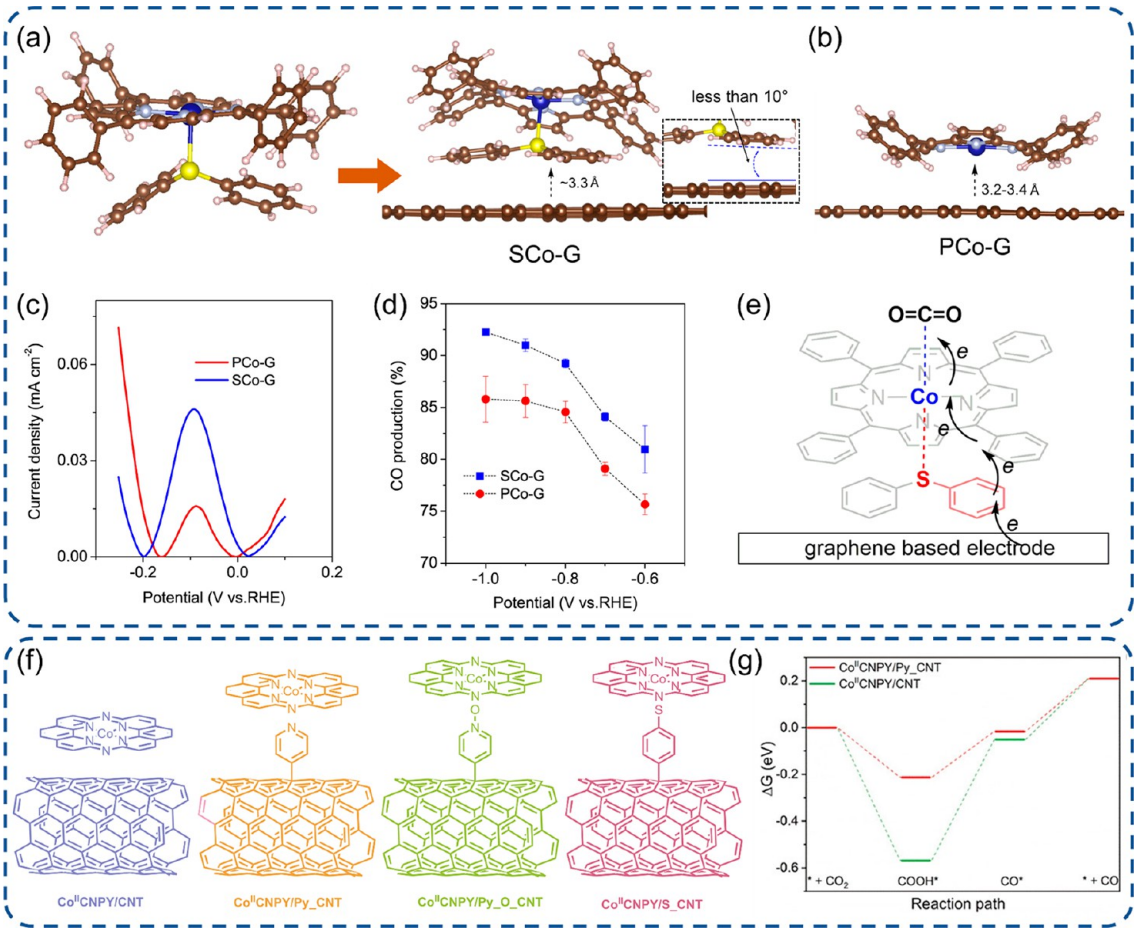

Figure 4. Engineering of SACs with axial functionalization. (a, b) PCo immobilized on graphene with or without diphenyl sulfide functionalization, (c) current density in differential pulse voltammograms for $[PCo]^-$ to PCo oxidation, (d) Faradaic efficiencies of CO production, and (e) a possible electron transfer pathway.[37] (f) Immobilization of Co^{II}CNPY on CNTs with diverse ligand axial functionalization and (g) free energy profiles for the CO_2RR.[102] (a-e) Reproduced with permission from ref 37. Copyright 2020 Wiley-VCH. (f-g) Reproduced with permission from ref 102. Copyright 2021 Wiley-VCH.

such challenges via compressive strain engineering, Yao et al. designed Ru SACs located on a $PtCu_x$ alloy to investigate the compressive strain effect on its OER activity under acidic conditions.[85] The sequential acid etching and electrochemical leaching treatment were adopted to precisely vary the substrate lattice parameter following Vegard's law and induce compressive strain.[71,86] The applied strain on Ru SACs not only optimized the oxygen binding affinity with the upshift of the *d*-band center of Ru toward the Fermi level but also suppressed the overoxidation of surface Ru during the OER with the alloys acting as electron tanks. Therefore, the regulation of binding strength and Ru electron states contributed to a volcano peak of Ru/Pt_3Cu SACs, showing a much lower overpotential and higher catalyst stability in comparison to commercial RuO_2.

Spin-State Tuning Engineering. An important catalytic descriptor for transition metal electrocatalytic materials, especially Fe, Co, and Ni, is that they possess partially filled *d* orbitals, which enable them to have a variable oxidation state and coordination configuration.[34] This makes them a suitable catalytic candidate to bind and activate molecules. The well-known Sabatier principle points out that mild binding energy is a prerequisite for high activity.[87] Therefore, the induced foreign electrons into unoccupied *d* orbitals can moderate the binding strength with adsorbate and adjust the electrocatalytic activity. Toward that, considerable efforts have been devoted to exploiting the regulation of electronic structure and control of electron spin state. Herein, two examples of the adjustment of Fe and Co spin states were presented (Figure 3). First, Fe^{III} has three classified spin states with low spin state ($t_{2g}5\ e_g0$), medium spin state ($t_{2g}4\ e_g1$), and high spin state ($t_{2g}3\ e_g2$).[88] The medium configuration with one electron in the antibond orbital of d_z^2 renders a moderate interaction with both O_2 and resulting intermediates through the penetration into the antibond π-orbital of oxygen, but for the low or high spin state, the interaction is either too strong or too weak.[89] As a proof-of-principle, Wang et al. designed a structure with an axial Fe−O−Ti bridge bond on top of FeN_4−O−Ti and FeN_3O−O−Ti (Figure 3a).[90] The Fe^{III} spin state was tuned to the medium spin state from the low state as verified by Mössbauer spectroscopy and temperature-dependent magnetization results (Figure 3b,c). It exhibited a significant drop in the reaction energy barrier from 3.05 to 0.76 eV for the rate-determining step of *O to *OH based on DFT calculations for the ORR. Recently, the comparatively weak OER performance of $ZnCo_2O_4$ was illustrated due to its intrinsic semiconductor property, as the Co^{3+} active sites in octahedral structure present a solely low spin state ($t_{2g}6\ e_g0$) and localized electronic structure (Figure 3d).[91] Later on, Xu et al. reported a state-of-the-art and facile spin state tuning strategy to obtain a robust electrocatalyst $ZnCo_2O_4$, which shows high potential to address the slow kinetics and large

https://doi.org/10.1021/acsnano.2c06827
ACS Nano 2022, 16, 17572−17592

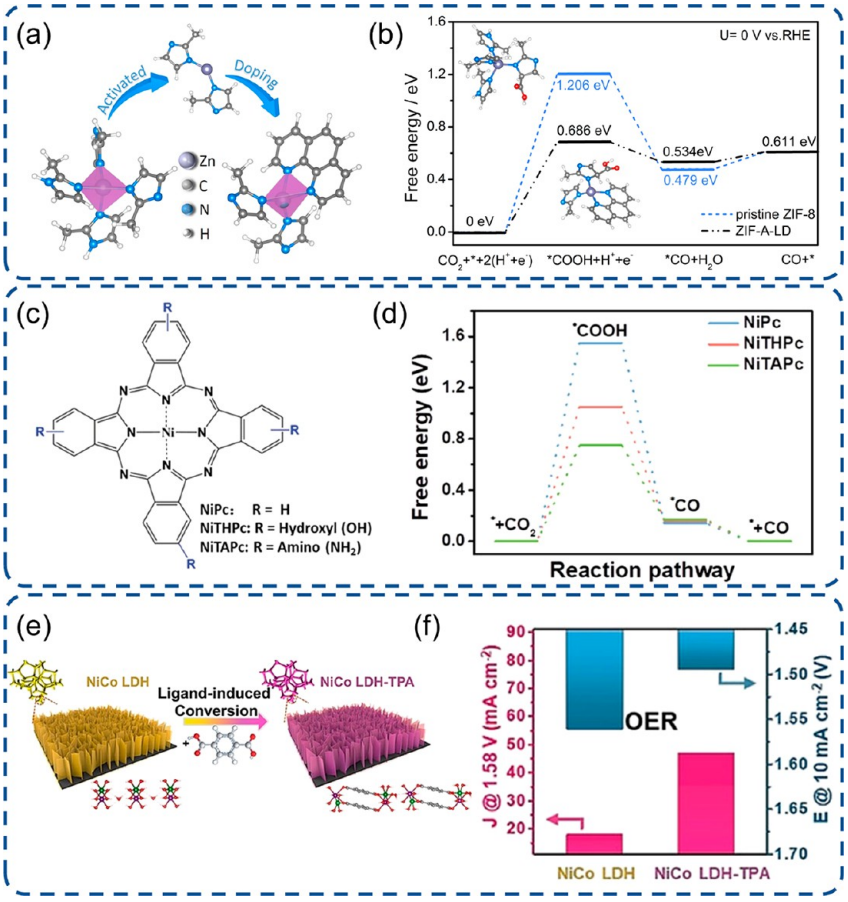

Figure 5. Engineering of SACs with ligand modification. (a) Schematic illustration of ZIF-8 doped by electron-donating phenanthroline and (b) free energy diagrams for the CO_2RR on doped ZIF-8.[39] (c) NiPc complex structure models with various substituents and (d) free energy diagrams for the CO_2RR showing the lowest barrier of NiPc with the electron-donating $-NH_2$ group.[108] (e) Schematic presentation of the ligand-induced conversion method and (f) the electrocatalytic activity in the OER before and after ligand modification.[117] (a-b) Reproduced with permission from ref 39. Copyright 2019 Wiley-VCH. (c-d) Reproduced with permission under a Creative Commons CC BY License from ref 108. Copyright 2021 the Authors. (e-f) Reproduced with permission from ref 117. Copyright 2021 Wiley-VCH.

overpotential in the OER.[92] With the facile control of synthetic calcination temperature, the octahedral lattice distortion was observed, and the configuration can be transformed from the low spin state to the medium ($t_{2g}5\ e_g1$) and high ($t_{2g}4\ e_g2$) spin states with controllable proportion (Figure 3e-h). This will propagate the delocalization of the electron and a spin-selected charge transport channel between Co and coordinated O from reactants. In addition, the unpaired electrons will also enhance the adsorption of molecules and reduce the reaction energy barrier.

Axial Functionalization Engineering. Macrocyclic complexes with one or more atoms on a single site anchored on supports are traditionally regarded as single site heterogeneous catalysts. They are included in this review as they bear similar metal sites as general SACs in terms of atomic configuration, whereas they show an advantage in terms of overall structure uniformity of catalytic sites compared to general SACs.[22,93] The axial functionalization, such as doping and polymer modification to generate an axial coordination, is demonstrated to be vital for macrocyclic complexes in electrocatalysis for the enhancement of catalytic activity, e.g., for CO_2 reduction.[94−96] Herein, the axial engineering mainly focused on the electrocatalysts based on macrocyclic complexes with mononuclear atoms serving as active sites in electrocatalysis. Kramer et al. studied a polymer functionalization of cobalt phthalocyanine, exhibiting a significant enhancement for CO_2RR activity due to the formed axial coordination configuration with a polymer.[97] Generally, porphyrin and phthalocyanine complexes exhibit a better proton reduction over CO_2 reduction in aqueous solutions. However, the Faradaic efficiency of H_2 can be significantly suppressed in the case of cobalt phthalocyanine via a formation of the Co−N axial coordination to pyridine. The reason was that the axial coordination can reduce Co(II) to a more nucleophilic Co(I), promote its binding with the Lewis acid CO_2, and enhance CO_2RR activity while suppressing proton reduction.

Wang et al. proposed an immobilization strategy for planar Co(II)-2,3-naphthalocyanine complexes (NapCo) on graphene by a doping treatment.[96] The treatment to graphene with sulfoxide and carboxyl dopants generates effectual sites to bind NapCo via the formation of the Co−O bond along the axial direction rather than pyridinic and pyrrolic N dopants which deliver weak van der Waals interactions. The intrinsic activity then can be improved via such an axial coordination formation and immobilization.[94,97] With the implementation in the CO_2RR under $KHCO_3$ solutions, the sulfoxide doped NapCo displays a much better efficiency than pristine NapCo, with 67.5% to 97% CO_2 Faradaic efficiency by varying the potential from −0.4 to −0.8 V. In addition, the charge transfer from the graphene substrate to Co sites was enhanced due to axial coordination, which was proved by a higher redox current of Co

https://doi.org/10.1021/acsnano.2c06827
ACS Nano 2022, 16, 17572−17592

ions via the $CoSO_4$/KCl probe.[98] It is well-known that the electron transfer between macrocyclic complexes and carbon substrate is critical in electrocatalysis, which can be amended via the molecular configuration, electron conjugation, and axial coordination. Recently, Wang et al. further realized the significant enhancement of electron transfer via the axial functionalization strategy by adding the diphenyl sulfide ligand as a relay molecule (Figure 4a-e).[37] The authors disclosed that the electrocatalyst with tetraphenylporphyrin cobalt (PCo) immobilized on graphene via $\pi-\pi$ stacking showed a poor redox activity for the CO_2RR, but the axial insertion of diphenyl sulfide between PCo and graphene yielded a higher current density and outstanding CO production (Figure 4c,d). Such a high performance stems from axial coordination which induced a stronger $\pi-\pi$ stacking interaction and better electron transfer. It was recognized that the porphyrin plane of the PCo on graphene tilted its tetraphenyl groups ~40° due to the steric effect of the neighboring porphyrin ring, but a face-to-face stacking configuration was established after axial modification with a much stronger $\pi-\pi$ interaction from the relay molecule (Figure 4a,b). Thus, an enhanced electron transfer was achieved, resulting in higher CO_2RR activity.[99,100] Later, with the view that carbon-based substrates normally contain multiple functional groups and it is difficult to identify the main contributor, Sun et al. immobilized cobalt complexes on CNTs covalently functionalized with specific groups to discern the main contributor for enhanced CO_2RR activity.[101,102] The axial coordination of Co to N in pyridine exhibited higher CO Faradaic efficiency and lower energy barriers than pristine, O-, S-functionalized pyridine in the CO_2RR (Figure 4f,g). Such an axial coordination enables the electron transfer to Co atoms and an increase of electron density as verified by XPS, leading to a stronger σ bond of Co−N.

Recently, Liu et al. summarized the axial coordination effect on SACs with a combination of experimental and theorical analyses with respect to the functionalization by chalcogen-, halogen-, and nitrogen-containing ligands.[103] Interestingly, axial engineering of Fe−N−C SACs was realized via the coordination of axial pyrrolic N in the N-doped graphene to FeN_4 with the formation of FeN_5.[104] The FeN_5 configuration was confirmed by Fe K-edge XANES spectra and DFT calculations, which yields significantly higher Faradaic efficiency in the CO_2RR and partial current density in comparison to FeN_4 SACs. The fundamental reason was revealed by theoretical analysis that the formed CO would be trapped on FeN_4 sites due to the strong binding, whereas the strength would be weakened in FeN_5 as the *d* electron in Fe centers would be transferred into *p* orbitals of axial pyrrolic N.

Ligand Engineering. The active sites with high electron density can effectively promote the activation of the CO_2RR, because it can enhance the transfer of electrons from active sites to the CO_2 antibonding orbital and subsequently combine with protons to generate the important intermediate *COOH.[105,106] Thus, the strategy to increase the electron density of active sites via ligand engineering is a possible pathway to elevate the activity. By doping the strong electron-donating ligand (1,10-phenanthroline) into ZIF-8, it enables an electron transfer to adjacent sp^2 C active sites. This can further facilitate the electron injection into the CO_2 antibonding orbital and realize the efficient electrochemical CO_2RR (Figure 5a,b).[39] Nickel phthalocyanine (NiPc) complex electrocatalysts suffer from poor electrocatalytic activity and durability.[107] With the alternation of flexible ligands of the NiPc complex by electron-donating moieties, Chen et al. unveiled a breakthrough in both CO_2RR activity and stability, especially using $-NH_2$ groups (Figure 5c).[108] The strong electron-donating feature of amino or hydroxyl groups yields a high electron density around the Ni nuclei, strengthens its interaction with CO_2, and reduces the free energy change of intermediate *COOH formation (Figure 5d).[109,110] Structural characterization illustrated that the $Ni-N_4$ active sites can be hydrogenolyzed during the reduction process, inducing a rupture of $Ni-N_4$ coordination in Pc ligands and formation of metal or its oxides. However, the appended electron-donating group on the $Ni-N_4$ ligands will induce an increase of $Ni-N_4$ reduction potentials, hamper its hydrogenolysis, and improve its structural stability.[110,111] Thus, good CO_2RR activity and stability can be coachieved via ligand engineering induced electron donation into active sties.

To further support the distinction of electron-donating moieties, an electron-withdrawing moiety *tert*-butyl group was also introduced into the NiPc flexible ligand.[108,110,112] As expected, the electron density decreased, and both CO_2RR activity and CO Faradaic efficiency are worse than pristine NiPc, NH_2-, or −OH modified NiPc. In addition, Zhang et al. also reported that the CO_2RR efficiency was obviously decreased after modification by strong electron-withdrawing cyano (−CN) groups but improved by electron-rich methoxy group modification.[110] Mukerjee gave a fundamental illustration for this phenomenon that e_g-orbitals (d_z^2) exhibit a downshift due to the electron-withdrawing effect and subsequently induced an anodic shift of redox potential for metal active sites.[80,113] As the electrocatalytic performance is highly related to the metal redox states, the electroreduction efficiency dropped accordingly.[36] This ligand engineering and understanding of the mechanism could be meaningful for the design of efficient catalysts for electrocatalytic reduction processes, such as the ORR and CO_2RR, but in some cases, the electron-withdrawing group may also bring a benefit from the electrocatalytic activity, such as in the case of the layered double hydroxide with a strong adsorption nature.[114,115] As the interaction is too strong between 3*d*-block metal sites and reaction intermediates, the performance of 3*d*-block metal catalysts is always unsatisfactory because of scaling relations.[116] Applying ligand exchange from the electron-donating −OH to the electron-withdrawing terephthalic acid group for the NiCo layered double hydroxide, Liu reported that the OER activity can be improved 5.7-fold (Figure 5e-f).[117] This improvement relies on the downshift of the *d*-band of the Co−Ni metal active sites and the increase of its electrophilicity after an electron-withdrawing ligand exchange, which induced a moderation of binding strength and a decrease of charge-transfer energy via a narrowed energy gap between adsorbed oxygen and metal sites.

Porosity Engineering. The relatively limited pore size in micropores of electrocatalysts and small openings with less than 2 nm, together with a noninterconnected porous structure, may restrict the transport of protons and reactant molecules during the reaction process and impair the electrocatalytic activity.[118] Although the mass transport capability is usually not a concern under low current density conditions in electrocatalysis, it is a critical factor and can be more important than metal sites under industry-relevant current density of over 100 mA per cm^2.[119,120] To overcome these drawbacks, porosity engineering has drawn extensive attention, aiming to achieve a large specific surface area with more exposed active sites, connected porous architecture for easy electrolyte penetration, and enhanced mass transport. Furthermore, the mesoporous structure can also facilitate the

https://doi.org/10.1021/acsnano.2c06827
ACS Nano 2022, 16, 17572−17592

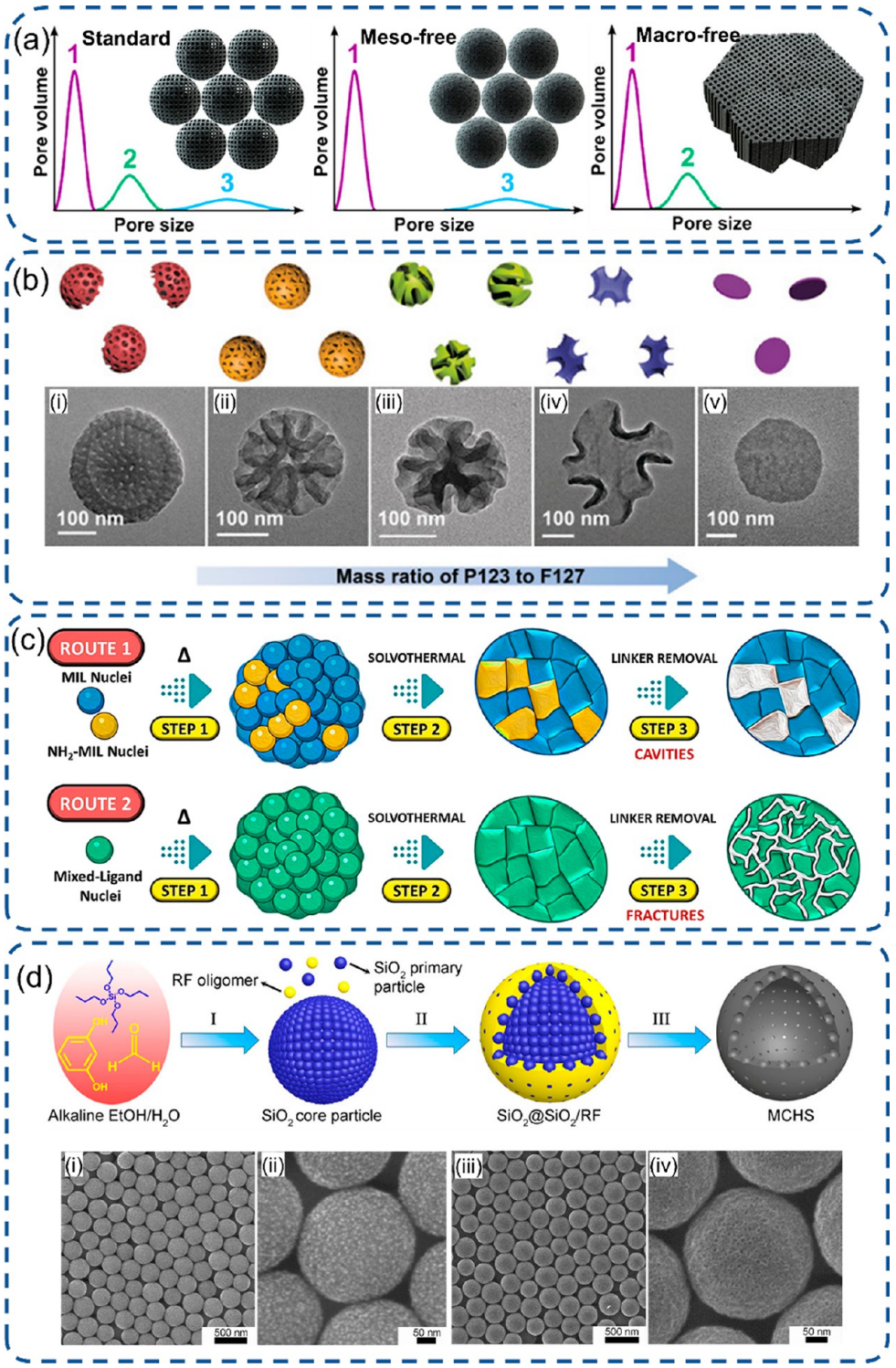

Figure 6. Engineering of SACs with the porous structure by soft or hard templates. (a) Representation of the three catalysts with a controllable pore system using the F127 soft template.[124] (b) Schematic illustration of the mesoporous evolution varying soft-template ratio of P123/F127 and corresponding TEM images.[35] (c) Synthesis mechanism for the porous structure via two routes of the ligand mixture.[130] (d) SiO_2 from TPOS as a hard template to generate mesoporous hollow spheres and SEM images of particles (i) and (ii) before and (iii) and (iv) after removing SiO_2.[135] (a) Reproduced with permission from ref 124. Copyright 2019 American Chemical Society. (b) Reproduced with permission from ref 35. Copyright 2018 Wiley-VCH. (c) Reproduced with permission under a Creative Commons CC BY License from ref 130. Copyright 2022 the Authors. (d) Reproduced with permission from ref 135. Copyright 2016 American Chemical Society.

removal of formed metal nanoparticles in substrates during the traditional acid etching process for the synthesis of SACs, which is much harder for nonporous materials.[121] The soft and hard templates are two main strategies to achieve the desired porous structure, but they still suffer from various issues, such as being time-consuming, nonuniform, and complicated for the hard-template process and costly and difficult to find suitable surfactants for soft-template process.[122] Thus, further efforts

https://doi.org/10.1021/acsnano.2c06827
ACS Nano 2022, 16, 17572−17592

are needed to explore a suitable strategy to overcome the drawbacks and obtain a tailored porous structure for electrocatalysis.[123]

Hyeon et al. designed a controllable pore size distribution strategy using soft templates and comprehensively investigated the individual contributions from mesopores and macropores.[124] The phenol and melamine resins are chosen as carbon and nitrogen precursors to be copolymerized first, followed by mixing with the F-127 polymer as the soft template.[125] Then, three ordered porous carbon Fe−N−C electrocatalysts were synthesized with micro-, meso-, or macropores (Figure 6a). A quantitative analysis was implemented via measurement of electric double-layer capacitance for the electrochemical surface area and relaxation time constant for ion transport capability. The authors discovered that the mesopores are the key parameter for the electrolyte wetting of the catalyst surface, while the macropores are responsible for the kinetic access to active sites residing inside micropores with minimizing the mass transport resistances. Eventually, a high ORR catalytic activity of a Fe−N−C electrocatalyst was achieved via porosity engineering. With facile dual-soft-template porosity engineering, Lou et al. developed macro/mesoporous carbon materials with walnut morphology features using a controllable assembly of surfactants (P123 and F127), polydopamine oligomers as the N-doped carbon precursor, and a pore swelling agent (1,3,5-trimethylbenzene).[35] P123 has the same hydrophobic moieties as F127 but a shorter hydrophilic headgroup. Meanwhile, the mesoporous structures are highly related to the hydrophilic−hydrophobic balance of such an amphiphilic block copolymer, and large curvature mesopores are favored for a high hydrophilic ratio.[126,127] Thus, the porous feature can be regulated with the increase of the mass ratio of P123 to F127 to generate various porous structures, from bowl-like morphology with 2D hexagonal pores to walnut particles with bicontinuous pore channels and even a nonporous lamellar structure (Figure 6b). Due to the high surface area and large mesochannels, the walnut carbon materials exhibit improved ORR activity in alkaline conditions. With the help of the cetyltrimethylammonium bromide (CTAB) surfactant and its subsequent etching by tannic acid, hollow mesoporous Co SACs can be synthesized on MOF derived carbon substrates achieving enhanced mass transport and eliminating dead zones located at the center of materials.[75,128]

Nowadays, MOFs as hard templates are broadly utilized to form a carbon based electrocatalyst with an adjustable porous structure. Selective removal of linker is one of the approaches to get a hierarchical structure for MOF derived materials based on the difference in linker thermolability.[129] Eder et al. projected a ligand removal strategy to introduce mesopores into the MOF structure.[130] The MOF was first synthesized with two mixed linkers. Then, the mesopores can be formed via the pyrolysis process when the onset decomposition temperature of the linker increases with more amino content. Finally, a 3D pore connectivity was achieved after pyrolysis treatment and selective removal of linkers (Figure 6c). In addition, carbon materials with large pores can be synthesized from the oxygen-rich MOFs by pyrolysis in comparison to an oxygen-poor precursor, which is owed to the evaporation of Zn (~908 °C) and formation of a large amount of gases such as CO_2 and H_2O during the pyrolysis process.[131] Ye et al. constructed a nitrogen-doped porous carbon (NPC) from the oxygen-rich Zn-MOF-74 precursor, and 10 nm large mesopores with rod-like morphology were clearly identified.[132] Prominent CO_2RR activity then was obtained, attributing to the promoted mass transport and more exposed active sites. SiO_2 colloid nanospheres, as another hard template, can be used as the core to form core−shell composite nanostructures. Followed by NaOH or HF etching, the SiO_2 core can be removed, and the mesopores then can be constructed. Li et al. proposed a hard-template Lewis acid doping strategy to synthesize Pd SACs using commercial SiO_2 as the pore-inducing hard template with a diameter around 20 nm to create the equal size mesopores.[133] Liang et al. also adopted SiO_2 to create mesopores, together with the NH_3 treatment to generate micropores to engineer meso/microcarbon materials with a 1280 m^2/g surface area in comparison to only 40 m^2/g for the counterpart without the silica template.[134] The high-porosity features lead to a high surface area and large amount of exposed active sites, which enables the catalyst to have a great ORR performance with a 0.83 V peak potential and 0.87 V half-wave ($E_{1/2}$) potential in comparison to the nonporous counterpart with a 0.56 V peak potential. The Dai and Yu groups proposed a silica-assisted strategy to generate mesoporous carbon hollow spheres involving the condensation of tetrapropyl orthosilicate (TPOS) or tetraethylorthosilicate (TEOS) and polymerization of resorcinol−formaldehyde (RF).[135,136] TPOS was first hydrolyzed via the Stöber process to synthesize the primary SiO_2 particles, and the formed primary SiO_2 particles were self-assembled to generate the SiO_2 large core structure. Due to the high ratio of TPOS to RF, the heterogeneous nucleation of RF was amended to a growth on SiO_2 core particles together with the co-condensation of SiO_2 primary small particles. After removal of SiO_2, the large mesopores of core and hollow pores from SiO_2 primary particles were created, with a controllable carbon sphere of 180−850 nm and hollow size from microscale to 14 nm (Figure 6d).

Although the introduced porosity may also affect the coordination configuration of SACs, it was rarely reported, and the main contribution to activity was still attributed to the enhanced mass transport. In an example of nitrogen coordinated Ni SACs, three mesoporous structures were introduced by adopting three SiO_2-based hard templates to achieve Ni SACs with 2D or 3D mesoporous channels.[119] The XPS results presented an obvious difference for the ratio of four N species in Ni SACs led by different mesoporous structures, namely pyridinic N, pyrrolic N, graphitic N, and oxidized N. However, their intrinsic activities are quite similar as verified at low current density in the CO_2RR. This may be due to the much larger amount of N in comparison to Ni metals in the matrix, whereas their catalytic performance is significantly different at high current density, especially for Ni SACs with 3D mesoporous channels presenting the highest CO_2-to-CO rate. This can be explained by the critical mass transport capability induced by mesopores.

TAILORING STRATEGIES ON ACTIVE SITES VIA A SYNERGISTIC EFFECT AND BINUCLEAR CONFIGURATION

The single atoms in the achieved SACs are commonly dispersed in random conditions or isolated from each other with a lack of interaction among active sites.[137] The synergetic interaction among them can potentially enhance the intrinsic activity of metal sites and stability of electrocatalysts,[138] such as in the case of the $Ni_2Fe(CN)_6$ electrocatalyst where an enhanced urea oxidation and limited transformation of catalysts were explained by the synergetic effect of Ni and Fe sites.[139] Therefore, a collective effect of metal−metal sites, namely correlated SACs

https://doi.org/10.1021/acsnano.2c06827
ACS Nano 2022, 16, 17572−17592

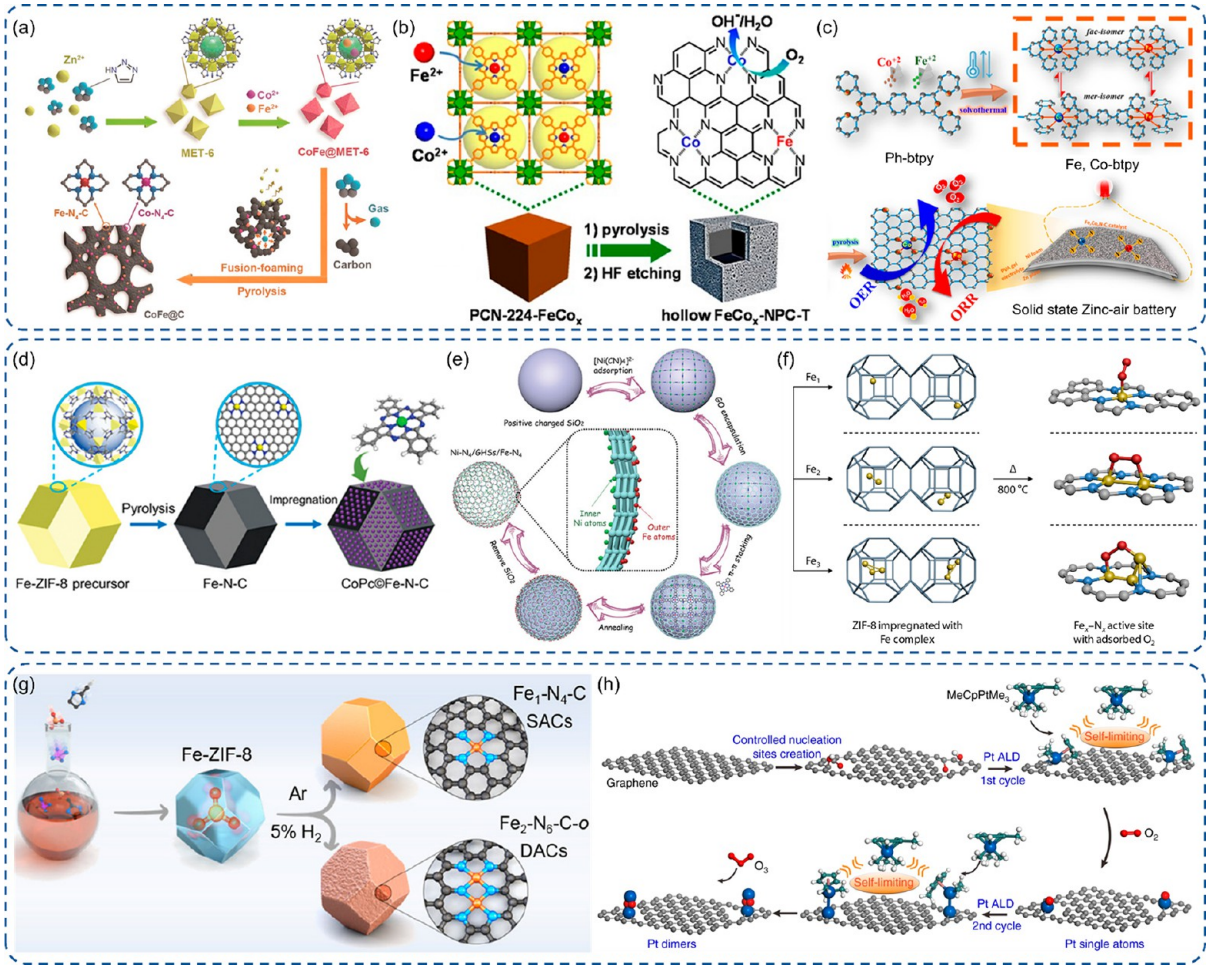

Figure 7. Engineering of active sites with binuclear strategies. (a-e) Schematic presentation for the stepwise synthesis of Co−Fe and Fe−Ni simple DACs.[151−153,156,157] (f, g) Schematic illustration of the synthesis of Fe−N/C with a controllable Fe_1, Fe_2, or Fe_3 configuration.[158,160] (h) Schematic proposal of the ALD synthesis of Pt_2−C catalysts with two cycles.[162] (a) Reproduced with permission from ref 151. Copyright 2019 Wiley-VCH. (b) Reproduced with permission from ref 152. Copyright 2017 Wiley-VCH. (c) Reproduced with permission from ref 153. Copyright 2022 American Chemical Society. (d) Reproduced with permission from ref 156. Copyright 2019 Wiley-VCH. (e) Reproduced with permission from ref 157. Copyright 2020 Wiley-VCH. (f) Reproduced with permission from ref 158. Copyright 2019 Elsevier. (g) Reproduced with permission from ref 160. Copyright 2022 American Chemical Society. (h) Reproduced with permission under a Creative Commons CC BY License from ref 162. Copyright 2017 the Authors.

(C-SACs), has attracted increasing attention.[140,141] This synergetic interaction can readily adjust their electronic structures by changing the level of orbital hybridization and antiorbital filling, which are highly related to the intrinsic electrocatalytic activity.[142,143] For example, Ir C-SACs were synthesized with the integration of Ir atoms into the framework of the cobalt oxide host offering great corrosion resistance and OER activity.[141] Including the metal−support interaction, an Ir−Ir short-range order can be identified by HAADF-STEM and pair distribution function analysis. The electronic structure analysis together with partial DOS simulation revealed that the Ir−Ir interaction has a fundamental influence on the electronic structure of active sites, specifically the position of the *d*-band and valence band. Adopting the previously reported precursor-dilution method and chelating properties of polypyrrole, Jin et al. synthesized Fe−N_4 SACs on carbon supports with a controllable distance of Fe−Fe sites.[46,144] After a systematic analysis, they demonstrated that the boosted ORR electrocatalytic activity and enhanced intrinsic activity of Fe sites stemmed from a strong interaction and synergetic effect when the d_{site} between Fe atoms was below 1.2 nm, reaching an optimum at 0.7 nm.

In comparison to SACs, DACs are very different in terms of the coordination environment and charge density.[24,145] With innate synergistic interaction in DACs, it has been an emerging frontier aiming to utilize the multiple active sites or positive synergistic effect to realize efficient catalysis, especially for the multistep processes of the OER and ORR.[146,147] Although DACs witnessed only a short period of development, substantial progress has been achieved in both experimental and theoretical fronts in terms of the synthesis strategies for precise control of the structure at the atomic level and regulation of electronic states, *d*-band center, and adsorption nature of active sites.[21,24,147−149] Generally, DACs can be classified into three categories according to the atomic configuration and metal types: simple DACs with a random mixture of two isolated atom sites in a single support, homonuclear DACs with only one type of metal forming pair atom sites, and heteronuclear DACs comprising different types of metals to form bimetal pairs.

https://doi.org/10.1021/acsnano.2c06827
ACS Nano 2022, 16, 17572−17592

DESIGN AND SYNTHESIS OF SIMPLE DACS

As aforementioned, MOF is a great substrate to derive SACs with M-N_4 coordination.[21] Therefore, simple DACs can be straightforwardly obtained using a mixture of two metal precursors. By applying a facile adsorption−calcination strategy on the carbon matrix derived from ZIF-8 with a mixture of $Fe(acac)_3$ or $Co(acac)_3$, simple Fe−Co DACs were synthesized with random distribution of single atom sites.[150] The simple Fe−Co DACs can also be obtained with one-step pyrolysis of MOF, together with metal precursors.[151] When a triazole-rich ligand, such as 1*H*-1,2,3-triazole, was used, the porous carbon was formed via fusion-foaming during the pyrolysis due to the considerable amount of gases generated (Figure 7a). The enhanced ORR performance is due to the increased active sites and synergy of adjacent FeN_4 and CoN_4 by chance. The high catalytic stability is due to the stabilization from the MOF derived porous carbon matrix. The porphyrinic MOF, like PCN-224, is a suitable candidate to metalate Fe and Co ions with an adjustable ratio.[152] After applying pyrolysis for graphitization and HF etching for removing metal particles, Fe−Co simple DACs can be generated with the optimized Fe/Co ratio of 1:2 (Figure 7b). Because of the bimetallic synergetic effect and highly porous carbon matrix, extraordinary ORR activity and stability were realized in both acidic and alkaline electrolytes. Sarkar et al. also reported a Fe−Co simple DAC using 4′,4‴′-(1,4-phenylene)bis(2,2′,6′,2″-terpyridine) to chelate Fe and Co ions followed by pyrolysis to form isolated FeN_4 and CoN_4 sites (Figure 7c).[153] The synergistic effect indued a downshift of *d*-band centers for both Co and Fe atoms, which can weaken the adsorption strength of intermediates and reduce the over-potential for both the OER and ORR. Thus, a high power density and stability can be achieved in the applied zinc−air batteries. With the introduction of the trimodal-porous structure, Zhu et al. manipulated a simple DAC comprising FeN_4 and NiN_4 on the MOF derived porous carbon substrate.[154] The DACs exhibited an outstanding ORR performance overweighting corresponding SACs and even benchmark Pt/C due to the collective optimization of active sites and mass transport. The trimodal porous structure was generated using polystyrene spheres (PSs) as a template to form ordered 3D PS monoliths.[155] Furthermore, Lin et al. designed a Co−Fe simple DAC by anchoring cobalt phthalocyanine on FeN_4 SACs via a simple wet chemical impregnation method (Figure 7d).[156] The Co−Fe simple DAC displayed a high CO Faradaic efficiency and 10-fold CO current density enhancement in the CO_2RR process in comparison to the corresponding Fe−N−C SACs. The significant improvement was also observed for a long-term stability test in terms of total current density and CO Faradaic efficiency, which is explained by the synergistic effect on the adsorption strength of intermediates and regulation of CO desorption. Recently, Chen and coauthors designed an interesting Janus hollow graphene shell with inner isolated Ni atoms and outer Fe single atoms.[157] The Ni−Fe simple DACs were synthesized via a 5-complex-type procedure following mainly the electrostatic attraction interaction, encapsulation, $\pi-\pi$ stacking interaction, and finally pyrolysis (Figure 7e). This electrocatalyst exhibits a bifunctional capability with high activity for both ORR and OER processes due to outer FeN_4 and inner NiN_4, respectively.

DESIGN AND SYNTHESIS OF HOMONUCLEAR DACS

As the intrinsic activity and electronic states of active sites can be remarkably affected by synergy from adjacent atom, a great deal of attention has been drawn to generate homoatomic pairs for a practical electrocatalysis application. In that regard, Sa et al. reported a Fe_2−N-C electrocatalyst with Fe_2 pairs confined in N-doped carbon substrates.[158] It was simply synthesized by the encapsulation of a binuclear $Fe_2(CO)_9$ precursor in the cavity of ZIF-8, followed by pyrolysis. In addition, the Fe SACs or even the Fe_3 triple atom catalyst can be achieved when $Fe(acac)_2$ or $Fe_3(CO)_{12}$ is adopted instead of $Fe_2(CO)_9$ (Figure 7f). The excellent ORR performance is owing to the alternative configuration of adsorbed O_2 from superoxo-like to peroxo-like ions induced by Fe_2 pairs.[159] Although the stability and corrosion resistance of Fe−N−C are still unsatisfactory in comparison to Pt/C under acidic conditions in the ORR, the obtained Fe_2−N-C DACs delivered an excellent durability under 0.5 M H_2SO_4 electrolytes with a slight decay and trace level of dissociation of the Fe−Fe bond after 20,000 continuous cycles with a 50 mV/s sweep rate at 0.6−1.0 V in the ORR. Recently, Wang also proposed Fe_2−N-C DACs with the introduction of $Fe(acac)_3$ into ZIF-8.[160] The tuning of Fe coordination can be simply achieved via pyrolysis atmosphere control (Figure 7g). In comparison to Fe SACs and Fe_2 pairs with FeN_3 coordination, the Fe_2 pairs with FeN_4 coordination exhibited the best CO_2RR activity because of the moderate *CO bonding strength proved by DFT calculation. The morphology and local structure of Fe_2−N-C DACs can be retained after a 21-h CO_2RR test, and ∼96% selectivity to CO can be retained. The atomic layer deposition (ALD) technique offers a great opportunity to manipulate the catalyst at the atomic level, as the self-limiting character can be achieved with "ALD window" regimes.[161] This surface self-limiting feature is highly suitable for the synthesis of SACs and DACs. Yan et al. reported the synthesis of Pt homonuclear DACs through the implementation of ALD with two cycles.[162] The defects were created first on graphene via acid oxidation as nucleation sites to anchor Pt atoms with the removal of ligands by oxidation. Subsequently, the second Pt atom was chemisorbed on primary isolated Pt sites with a one-to-one coordination due to ligand restrictions. The main factors to avoid the formation of particles were complete elimination of oxygen-contained groups on graphene and low ALD temperature (Figure 7h). The production of C_{2+} chemicals in the CO_2RR is realized on Cu active sites in electrocatalysis, and the manipulation of Cu_2 pairs deserves an in-depth study.[163] Li et al. constructed Cu homonuclear DACs via two steps, the fabrication of $Cu(BTC)(H_2O)_3$ MOF and subsequently thermal treatment together with dicyandiamide as the nitrogen source.[164] The high selectivity to C_{2+} chemicals is explained by the adjacent adsorption of two *CO intermediates.

DESIGN AND SYNTHESIS OF HETERONUCLEAR DACS

Although it remains a substantial challenge to contrast heteronuclear DACs with one-to-one pairs, many researchers strive to devote their efforts in structure design and theoretical calculation to seize the opportunity for utilizing a positive synergistic effect and modulation of electronic structures induced by different electronegativities to achieve enhanced intrinsic activity.[165] Based on a strategy named preconstrained metal twins, Fe−Co DACs were synthesized with a preformation of FeCo binuclear phthalocyanines and subsequent encapsulation inside ZIF-8 cages (Figure 8a).[166] It

https://doi.org/10.1021/acsnano.2c06827
ACS Nano 2022, 16, 17572−17592

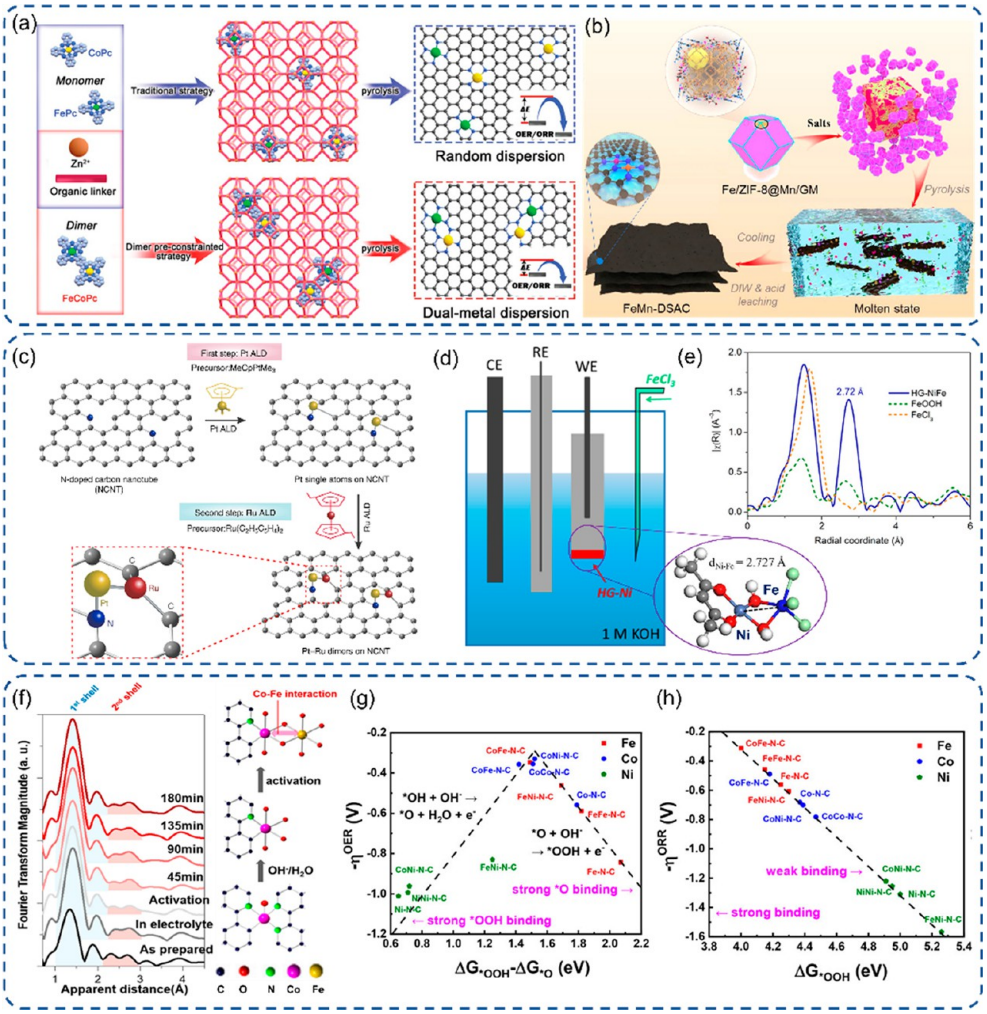

Figure 8. Engineering of active sites with heteronuclear strategies. (a-d) Schematic presentation for the formation of Fe−Co, Fe−Mn, Pt−Ru, and Ni−Fe heteronuclear DACs.[166,167,171,172] Fourier-transformed EXAFS spectra of (e) Fe K-edge after activation[172] and (f) Co K-edge of Co−N−C with various durations in the OER.[174] (g, h) DFT calculation results on M_2N_6 DACs for the ORR overpotential versus ΔG*OOH and the OER overpotential versus adsorption free energy difference (ΔG*OOH − ΔG*O).[175] (a) Reproduced with permission from ref 166. Copyright 2022 Wiley-VCH. (b) Reproduced with permission from ref 167. Copyright 2022 Wiley-VCH. (c) Reproduced with permission under a Creative Commons CC BY License from ref 171. Copyright 2019 the Authors. (d-e) Reprinted with permission from AAAS and distributed under a Creative Commons CC BY-NC 4.0 License from ref 172. Copyright 2018 the Authors, some rights reserved; exclusive licensee AAAS. (f) Reproduced with permission from ref 174. Copyright 2019 American Chemical Society. (g-h) Reproduced with permission from ref 175. Copyright 2022 American Chemical Society.

exhibited a better activity than corresponding Fe or Co SACs in both OER and ORR processes. The practical application in liquid Zn−air batteries and flexible all-solid-state batteries was realized with good rechargeability. Li et al. reported Fe−Mn DACs on layered graphene nanosheets with 62% pairs and 38% single atoms via statistical analysis.[167] The Fe atoms were easily encapsulated in ZIF-8, while Mn atoms were simply chelated on the Fe/ZIF-8 surface by the glucose-melamine complex (Figure 8b). The salts were mixed before pyrolysis, which are key factors to form layered graphene and Fe−Mn pairs.[168,169] The Fe−Mn DACs showed great stability with negligible decay after 10000 continuous CV cycles in both alkaline and acidic conditions for the ORR. Following an encapsulation strategy during the preparation of MOFs, Liu et al. synthesized Ru-M (M = Fe, Co, Ni) DACs. The newly formed Co−Ru bond can be identified by XANES and EXAFS with $RuCoN_6$ configuration.[19,170] Coupled with *d*-block metals with an electron-donating nature, the electronic state of Ru atoms can be modulated giving a balance of its strong adsorption nature for reactants in the ORR. Thus, an excellent ORR performance can be realized after the optimization of *d*-block metals. With the application of the atomic layer deposition technique, the Pt−Ru DACs were successfully synthesized on CNTs (Figure 8c).[171] Pt atoms were first anchored on CNTs to form Pt SACs. Then, Ru atoms were selectively attached on the Pt atoms during the second ALD cycle due to much lower adsorption energy with the final formation of 70% dimers in the catalysts. Due to the synergetic effect and electron redistribution from Ru to Pt, the obtained Pt−Ru DACs yielded good stability and a 54-fold mass activity enhancement in the HER with respect to Pt/C.

Recently, Wang et al. designed a Ni−Fe heteronuclear DAC via an *in situ* electrochemical method during the OER process (Figure 8d,e).[172] The single Ni atoms were first anchored on graphene, followed by application of cyclic voltammetry in the KOH solution containing Fe species. The parent Ni SACs displayed poor OER activity, but the subsequent formation of

https://doi.org/10.1021/acsnano.2c06827
ACS Nano 2022, 16, 17572−17592

Ni−Fe pairs yields a significant enhancement of the OER performance with an almost 10-fold TOF improvement. This elevation may be attributed to the shift of a terminal geometry adsorption of HO^- ions on Ni atoms to a bridging geometry on Ni−Fe pairs proved by EXAFS.[173] Later, Bai and coauthors extended this *in situ* electrochemical method to the generation of Co−Fe pairs.[174] The Co SACs were first designed, followed by galvanostatic activation in the KOH solution containing Fe species. The overpotential at E_{10} was dropped to 309 mV after activation in comparison to 495 mV of the pristine one, while a new peak was identified at 2.51 Å assigned to Co−Fe bond formation in EXAFS spectra (Figure 8f). The Co−Fe DACs exhibited good stability and a slight increase in the overpotential indicated in both polarization curves after 3000 CV cycles and galvanostatic for 16 h at 10 mA/cm^2. More recently, Zhou et al. carried out a theoretical calculation to explore the synergy and adsorption strength of intermediates by modeling DACs with M_2N_6 configurations using Fe, Co, and Ni metals (Figure 8g,h).[175] Based on the results, a linear correlation was observed for the ORR overpotential versus adsorption free energy of ΔG*OOH, while a volcano feature was discovered for the OER overpotential versus the difference of adsorption free energy (ΔG*OOH − ΔG*O). The Co−Fe pairs showed the highest OER activity because of synergy-induced more efficient electron transfer.[176] Furthermore, the authors synthesized Co−Fe heteronuclear DACs via a two-step pyrolysis procedure, which exhibited a great OER performance as proof-of-concept of DFT results. The similar conclusion was summarized for Pt−Co DACs that the adjacent metals can induce an asymmetry distribution of electrons and alter the adsorption strength of intermediates.[177,178]

SUMMARY AND PERSPECTIVES

Owing to the unusual configuration and high atom utilization, SACs have emerged as efficient electrocatalysts for a wide range of applications, such as the HER, OER, ORR, CO_2RR, and so on, but the shortcomings are also obvious with low loading and monotonic sites. Herein, the synthesis of SACs was explored first based on carbon or non-carbon supports, which provide the matrix to anchor the single atoms and impact its electronic states. Subsequently, the recent advances in tailoring strategies and rational designs were systemically summarized in terms of electronic and geometric configurations to overcome the weakness of SACs. Strain engineering and spin-state tuning can alter the orbital position of single atoms with respect to the Fermi level and affect orbital overlapping to optimize the molecular adsorption strength and energy barriers. Axial functionalization and ligand engineering can enhance the charge transfer from support to active sites and amend the binding energy of intermediates via the electron-donating or withdrawing effect. Porosity engineering with either a soft or hard template can deliver an especial and interconnected structure with large specific surface area, maximization of exposed active sites, and improvement of mass transport efficiency. Lastly, the DACs with the pair atoms were discussed with three types: simple DACs and homo- and heteronuclear DACs. In comparison to SACs, DACs can increase the number of active sites and metal loadings and provide an adjustable electronic structure due to the adjacent atoms. Although substantial progress has been obtained, great challenges remain, and some perspectives are proposed as follows:

1) Groundbreaking strategies for tailoring the activity of SACs are desired, especially a delicate balance of the interaction with various intermediates to break the scaling relationship and enhance the intrinsic activity. This may make use of the theoretical calculation and simulation to achieve a fundamental understanding of effects derived from electronic and geometric configurations and obtain a breakthrough in the design of electrocatalysts.
2) Design of diverse active sites should be put forward to acquire a highly efficient electrocatalyst, especially with bifunctional activity for the OER and ORR. DAC is a reasonable alternative to SAC, but the development is just in its infancy in spite of the numerous reports. In comparison to the popular rigid DACs anchored mainly in a carbon matrix, the recent report of flexible dual atom sites may stimulate and lead to another research field for an outstanding electrocatalytic performance as the demonstration.[172] Furthermore, triple or quadruple atom sites with homo- or heteronuclear will be another interesting design to increase metal loading and utilize the synergetic effect.
3) *In situ* characterization to get insights into the nature of active centers is necessary and still lacking. As the real states of active sites are very complicated, the adsorbed species can induce the change of electronic states, and the high current density and potential can lead to an evolution of active sites. However, most of the powerful techniques are carried out as *ex situ* characterization in most of the research, such as XPS, HAADF-STEM, and XAFS. Although the understanding at an atomic level benefits greatly from DFT calculation and simulation, it may still have a large gap toward the real situation in working conditions. Through the *in situ* characterization and thorough understanding of the complicated active centers, the rational design and practical application of electrocatalysts will be output for a bright electrocatalysis future.

AUTHOR INFORMATION

Corresponding Authors

Xin Wang − *School of Chemical and Biomedical Engineering, Nanyang Technological University, Singapore 637459, Singapore; Cambridge Centre for Advanced Research and Education in Singapore Ltd (Cambridge CARES), Singapore 138602, Singapore;* orcid.org/0000-0003-2686-466X; Email: wangxin@ntu.edu.sg

Jong-Min Lee − *School of Chemical and Biomedical Engineering, Nanyang Technological University, Singapore 637459, Singapore;* orcid.org/0000-0001-6300-0866; Email: jmlee@ntu.edu.sg

Authors

Hongwei Zhang − *School of Chemical and Biomedical Engineering, Nanyang Technological University, Singapore 637459, Singapore; Cambridge Centre for Advanced Research and Education in Singapore Ltd (Cambridge CARES), Singapore 138602, Singapore*

Xindie Jin − *School of Chemical and Biomedical Engineering, Nanyang Technological University, Singapore 637459, Singapore*

Complete contact information is available at: https://pubs.acs.org/10.1021/acsnano.2c06827

https://doi.org/10.1021/acsnano.2c06827
ACS Nano 2022, 16, 17572−17592

Notes

The authors declare no competing financial interest.

ACKNOWLEDGMENTS

This project was supported by the National Research Foundation (NRF), Prime Minister's Office, Singapore, under its Campus for Research Excellence and Technological Enterprise (CREATE) program. We also acknowledge financial support from the academic research fund AcRF tier 1 (RG63/21), Ministry of Education, Singapore.

VOCABULARY

Strain engineering, compressive or tensile strain formed around active sites to vary the bond length and its electronic state for the tuning of electrocatalytic activity

Spin-state tuning engineering, strategies to manipulate the electron spin state of d-block atoms through the injection of foreign electrons into d orbitals to mainly control its adsorption nature

Axial functionalization engineering, generation of an axial coordination on active sites via doping, polymer modification, *etc*. to regulate the electronic state of active sites and electron transfer efficiency between active sites and supporting matrix

Ligand engineering, approaches to optimize the electronic state of active sites and its adsorption nature via utilization of electron donation or withdrawal nature of ligands

Porosity engineering, synthesis of porous structure via a soft and hard template aiming to achieve a large specific surface area with more exposed active sites, connected porous architecture for easy electrolyte penetration, and enhanced mass transport

REFERENCES

(1) Zhao, C.-X.; Liu, J.-N.; Wang, J.; Ren, D.; Li, B.-Q.; Zhang, Q. Recent advances of noble-metal-free bifunctional oxygen reduction and evolution electrocatalysts. *Chem. Soc. Rev.* **2021**, *50*, 7745−7778.

(2) Seh, Z. W.; Kibsgaard, J.; Dickens, C. F.; Chorkendorff, I.; Nørskov, J. K.; Jaramillo, T. F. Combining theory and experiment in electrocatalysis: Insights into materials design. *Science* **2017**, *355*, eaad4998.

(3) Chu, S.; Majumdar, A. Opportunities and challenges for a sustainable energy future. *Nature* **2012**, *488*, 294−303.

(4) Jose, V.; Nsanzimana, J. M. V.; Hu, H.; Choi, J.; Wang, X.; Lee, J.-M. Highly Efficient Oxygen Reduction Reaction Activity of N-Doped Carbon-Cobalt Boride Heterointerfaces. *Adv. Energy Mater.* **2021**, *11*, 2100157.

(5) Chen, Y.; Fan, Z.; Wang, J.; Ling, C.; Niu, W.; Huang, Z.; Liu, G.; Chen, B.; Lai, Z.; Liu, X.; Li, B.; Zong, Y.; Gu, L.; Wang, J.; Wang, X.; Zhang, H. Ethylene Selectivity in Electrocatalytic CO_2 Reduction on Cu Nanomaterials: A Crystal Phase-Dependent Study. *J. Am. Chem. Soc.* **2020**, *142*, 12760−12766.

(6) Huang, Z.-F.; Song, J.; Du, Y.; Dou, S.; Sun, L.; Chen, W.; Yuan, K.; Dai, Z.; Wang, X. Optimizing interfacial electronic coupling with metal oxide to activate inert polyaniline for superior electrocatalytic hydrogen generation. *Carbon Energy* **2019**, *1*, 77−84.

(7) Li, Y.; Zhang, S. L.; Cheng, W.; Chen, Y.; Luan, D.; Gao, S.; Lou, X. W. Loading Single-Ni Atoms on Assembled Hollow N-Rich Carbon Plates for Efficient CO_2 Electroreduction. *Adv. Mater.* **2022**, *34*, 2105204.

(8) Huang, Z.-F.; Xi, S.; Song, J.; Dou, S.; Li, X.; Du, Y.; Diao, C.; Xu, Z. J.; Wang, X. Tuning of lattice oxygen reactivity and scaling relation to construct better oxygen evolution electrocatalyst. *Nat. Commun.* **2021**, *12*, 3992.

(9) Li, L.; Tang, C.; Jin, H.; Davey, K.; Qiao, S.-Z. Main-group elements boost electrochemical nitrogen fixation. *Chem.* **2021**, *7*, 3232−3255.

(10) Liu, S.; Lu, X. F.; Xiao, J.; Wang, X.; Lou, X. W. Bi_2O_3 Nanosheets Grown on Multi-Channel Carbon Matrix to Catalyze Efficient CO_2 Electroreduction to HCOOH. *Angew. Chem., Int. Ed.* **2019**, *58*, 13828−13833.

(11) Huang, Z.-F.; Song, J.; Dou, S.; Li, X.; Wang, J.; Wang, X. Strategies to Break the Scaling Relation toward Enhanced Oxygen Electrocatalysis. *Matter* **2019**, *1*, 1494−1518.

(12) Huang, Z.-F.; Song, J.; Du, Y.; Xi, S.; Dou, S.; Nsanzimana, J. M. V.; Wang, C.; Xu, Z. J.; Wang, X. Chemical and structural origin of lattice oxygen oxidation in Co−Zn oxyhydroxide oxygen evolution electrocatalysts. *Nat. Energy.* **2019**, *4*, 329−338.

(13) Jiang, K.; Zhao, D.; Guo, S.; Zhang, X.; Zhu, X.; Guo, J.; Lu, G.; Huang, X. Efficient oxygen reduction catalysis by subnanometer Pt alloy nanowires. *Sci. Adv.* **2017**, *3*, e1601705.

(14) Tian, X.; Zhao, X.; Su, Y.-Q.; Wang, L.; Wang, H.; Dang, D.; Chi, B.; Liu, H.; Hensen, E. J. M.; Lou, X. W.; Xia, B. Y. Engineering bunched Pt-Ni alloy nanocages for efficient oxygen reduction in practical fuel cells. *Science* **2019**, *366*, 850−856.

(15) Zhang, S. L.; Lu, X. F.; Wu, Z.-P.; Luan, D.; Lou, X. W. Engineering Platinum-Cobalt Nano-alloys in Porous Nitrogen-Doped Carbon Nanotubes for Highly Efficient Electrocatalytic Hydrogen Evolution. *Angew. Chem., Int. Ed.* **2021**, *60*, 19068−19073.

(16) Wang, Y.; Wang, D.; Li, Y. Rational Design of Single-Atom Site Electrocatalysts: From Theoretical Understandings to Practical Applications. *Adv. Mater.* **2021**, *33*, 2008151.

(17) Zheng, X.; Li, P.; Dou, S.; Sun, W.; Pan, H.; Wang, D.; Li, Y. Non-carbon-supported single-atom site catalysts for electrocatalysis. *Energy Environ. Sci.* **2021**, *14*, 2809−2858.

(18) Zhang, J.; Xu, X.; Yang, L.; Cheng, D.; Cao, D. Single-Atom Ru Doping Induced Phase Transition of MoS_2 and S Vacancy for Hydrogen Evolution Reaction. *Small Methods* **2019**, *3*, 1900653.

(19) Xiao, M.; Zhu, J.; Li, G.; Li, N.; Li, S.; Cano, Z. P.; Ma, L.; Cui, P.; Xu, P.; Jiang, G.; Jin, H.; Wang, S.; Wu, T.; Lu, J.; Yu, A.; Su, D.; Chen, Z. A Single-Atom Iridium Heterogeneous Catalyst in Oxygen Reduction Reaction. *Angew. Chem., Int. Ed.* **2019**, *58*, 9640−9645.

(20) Zang, W.; Kou, Z.; Pennycook, S. J.; Wang, J. Heterogeneous Single Atom Electrocatalysis, Where "Singles" Are "Married. *Adv. Energy Mater.* **2020**, *10*, 1903181.

(21) Han, A.; Wang, B.; Kumar, A.; Qin, Y.; Jin, J.; Wang, X.; Yang, C.; Dong, B.; Jia, Y.; Liu, J.; Sun, X. Recent Advances for MOF-Derived Carbon-Supported Single-Atom Catalysts. *Small Methods* **2019**, *3*, 1800471.

(22) Wang, A.; Li, J.; Zhang, T. Heterogeneous single-atom catalysis. *Nat. Rev. Chem.* **2018**, *2*, 65−81.

(23) Jeong, H.; Shin, S.; Lee, H. Heterogeneous Atomic Catalysts Overcoming the Limitations of Single-Atom Catalysts. *ACS Nano* **2020**, *14*, 14355−14374.

(24) Li, R.; Wang, D. Superiority of Dual-Atom Catalysts in Electrocatalysis: One Step Further Than Single-Atom Catalysts. *Adv. Energy Mater.* **2022**, *12*, 2103564.

(25) Mehmood, A.; Gong, M.; Jaouen, F.; Roy, A.; Zitolo, A.; Khan, A.; Sougrati, M.-T.; Primbs, M.; Bonastre, A. M.; Fongalland, D.; Drazic, G.; Strasser, P.; Kucernak, A. High loading of single atomic iron sites in Fe−NC oxygen reduction catalysts for proton exchange membrane fuel cells. *Nat. Catal.* **2022**, *5*, 311−323.

(26) Xia, C.; Qiu, Y.; Xia, Y.; Zhu, P.; King, G.; Zhang, X.; Wu, Z.; Kim, J. Y.; Cullen, D. A.; Zheng, D.; Li, P.; Shakouri, M.; Heredia, E.; Cui, P.; Alshareef, H. N.; Hu, Y.; Wang, H. General synthesis of single-atom catalysts with high metal loading using graphene quantum dots. *Nat. Chem.* **2021**, *13*, 887−894.

(27) Wu, J.; Xiong, L.; Zhao, B.; Liu, M.; Huang, L. Densely Populated Single Atom Catalysts. *Small Methods* **2020**, *4*, 1900540.

(28) Wu, J.; Zhou, H.; Li, Q.; Chen, M.; Wan, J.; Zhang, N.; Xiong, L.; Li, S.; Xia, B. Y.; Feng, G.; Liu, M.; Huang, L. Densely Populated Isolated Single Co-N Site for Efficient Oxygen Electrocatalysis. *Adv. Energy Mater.* **2019**, *9*, 1900149.

https://doi.org/10.1021/acsnano.2c06827
ACS Nano 2022, 16, 17572−17592

(29) Tang, T.; Wang, Z.; Guan, J. Optimizing the Electrocatalytic Selectivity of Carbon Dioxide Reduction Reaction by Regulating the Electronic Structure of Single-Atom M-N-C Materials. *Adv. Funct. Mater.* **2022**, *32*, 2111504.
(30) Narendra Kumar, A. V.; Muthu Prabhu, S.; Shin, W. S.; Yadav, K. K.; Ahn, Y.; Abdellattif, M. H.; Jeon, B.-H. Prospects of non-noble metal single atoms embedded in two-dimensional (2D) carbon and non-carbon-based structures in electrocatalytic applications. *Coord. Chem. Rev.* **2022**, *467*, 214613.
(31) Kumar, P.; Al-Attas, T. A.; Hu, J.; Kibria, M. G. Single Atom Catalysts for Selective Methane Oxidation to Oxygenates. *ACS Nano* **2022**, *16*, 8557−8618.
(32) Liu, P.; Zhao, Y.; Qin, R.; Mo, S.; Chen, G.; Gu, L.; Chevrier, D. M.; Zhang, P.; Guo, Q.; Zang, D.; Wu, B.; Fu, G.; Zheng, N. Photochemical route for synthesizing atomically dispersed palladium catalysts. *Science* **2016**, *352*, 797−800.
(33) Calle-Vallejo, F.; Loffreda, D.; Koper, M. T. M.; Sautet, P. Introducing structural sensitivity into adsorption-energy scaling relations by means of coordination numbers. *Nat. Chem.* **2015**, *7*, 403−410.
(34) Chen, Z.; Niu, H.; Ding, J.; Liu, H.; Chen, P.-H.; Lu, Y.-H.; Lu, Y.-R.; Zuo, W.; Han, L.; Guo, Y.; Hung, S.-F.; Zhai, Y. Unraveling the Origin of Sulfur-Doped Fe-N-C Single-Atom Catalyst for Enhanced Oxygen Reduction Activity: Effect of Iron Spin-State Tuning. *Angew. Chem., Int. Ed.* **2021**, *60*, 25404−25410.
(35) Guan, B. Y.; Zhang, S. L.; Lou, X. W. Realization of Walnut-Shaped Particles with Macro-/Mesoporous Open Channels through Pore Architecture Manipulation and Their Use in Electrocatalytic Oxygen Reduction. *Angew. Chem., Int. Ed.* **2018**, *57*, 6176−6180.
(36) Wang, J.; Dou, S.; Wang, X. Structural tuning of heterogeneous molecular catalysts for electrochemical energy conversion. *Sci. Adv.* **2021**, *7*, eabf3989.
(37) Wang, J.; Huang, X.; Xi, S.; Xu, H.; Wang, X. Axial Modification of Cobalt Complexes on Heterogeneous Surface with Enhanced Electron Transfer for Carbon Dioxide Reduction. *Angew. Chem., Int. Ed.* **2020**, *59*, 19162−19167.
(38) Dai, Z.; Liu, L.; Zhang, Z. Strain Engineering of 2D Materials: Issues and Opportunities at the Interface. *Adv. Mater.* **2019**, *31*, 1805417.
(39) Dou, S.; Song, J.; Xi, S.; Du, Y.; Wang, J.; Huang, Z.-F.; Xu, Z. J.; Wang, X. Boosting Electrochemical CO_2 Reduction on Metal−Organic Frameworks via Ligand Doping. *Angew. Chem., Int. Ed.* **2019**, *58*, 4041−4045.
(40) Peng, Y.; Lu, B.; Chen, S. Carbon-Supported Single Atom Catalysts for Electrochemical Energy Conversion and Storage. *Adv. Mater.* **2018**, *30*, 1801995.
(41) Ye, C.; Zhang, N.; Wang, D.; Li, Y. Single atomic site catalysts: synthesis, characterization, and applications. *Chem. Commun.* **2020**, *56*, 7687−7697.
(42) Qiao, B.; Wang, A.; Yang, X.; Allard, L. F.; Jiang, Z.; Cui, Y.; Liu, J.; Li, J.; Zhang, T. Single-atom catalysis of CO oxidation using Pt_1/FeO_x. *Nat. Chem.* **2011**, *3*, 634−641.
(43) Dou, S.; Li, X.; Wang, X. Rational Design of Metal-Organic Frameworks towards Efficient Electrocatalysis. *ACS Mater. Lett.* **2020**, *2*, 1251−1267.
(44) Yin, P.; Yao, T.; Wu, Y.; Zheng, L.; Lin, Y.; Liu, W.; Ju, H.; Zhu, J.; Hong, X.; Deng, Z.; Zhou, G.; Wei, S.; Li, Y. Single Cobalt Atoms with Precise N-Coordination as Superior Oxygen Reduction Reaction Catalysts. *Angew. Chem., Int. Ed.* **2016**, *55*, 10800−10805.
(45) Huang, J.; Li, Y.; Huang, R.-K.; He, C.-T.; Gong, L.; Hu, Q.; Wang, L.; Xu, Y.-T.; Tian, X.-Y.; Liu, S.-Y.; Ye, Z.-M.; Wang, F.; Zhou, D.-D.; Zhang, W.-X.; Zhang, J.-P. Electrochemical Exfoliation of Pillared-Layer Metal-Organic Framework to Boost the Oxygen Evolution Reaction. *Angew. Chem., Int. Ed.* **2018**, *57*, 4632−4636.
(46) He, X.; He, Q.; Deng, Y.; Peng, M.; Chen, H.; Zhang, Y.; Yao, S.; Zhang, M.; Xiao, D.; Ma, D.; Ge, B.; Ji, H. A versatile route to fabricate single atom catalysts with high chemoselectivity and regioselectivity in hydrogenation. *Nat. Commun.* **2019**, *10*, 3663.
(47) Han, A.; Chen, W.; Zhang, S.; Zhang, M.; Han, Y.; Zhang, J.; Ji, S.; Zheng, L.; Wang, Y.; Gu, L.; Chen, C.; Peng, Q.; Wang, D.; Li, Y. A Polymer Encapsulation Strategy to Synthesize Porous Nitrogen-Doped Carbon-Nanosphere-Supported Metal Isolated-Single-Atomic-Site Catalysts. *Adv. Mater.* **2018**, *30*, 1706508.
(48) Zhang, H.; An, P.; Zhou, W.; Guan, B. Y.; Zhang, P.; Dong, J.; Lou, X. W. Dynamic traction of lattice-confined platinum atoms into mesoporous carbon matrix for hydrogen evolution reaction. *Sci. Adv.* **2018**, *4*, eaao6657.
(49) Wang, J.; Gan, L.; Zhang, Q.; Reddu, V.; Peng, Y.; Liu, Z.; Xia, X.; Wang, C.; Wang, X. A Water-Soluble Cu Complex as Molecular Catalyst for Electrocatalytic CO_2 Reduction on Graphene-Based Electrodes. *Adv. Energy Mater.* **2019**, *9*, 1803151.
(50) Dou, S.; Sun, L.; Xi, S.; Li, X.; Su, T.; Fan, H. J.; Wang, X. Enlarging the π-Conjugation of Cobalt Porphyrin for Highly Active and Selective CO_2 Electroreduction. *ChemSusChem* **2021**, *14*, 2126−2132.
(51) Sun, L.; Huang, Z.; Reddu, V.; Su, T.; Fisher, A. C.; Wang, X. A Planar, Conjugated N_4-Macrocyclic Cobalt Complex for Heterogeneous Electrocatalytic CO_2 Reduction with High Activity. *Angew. Chem., Int. Ed.* **2020**, *59*, 17104−17109.
(52) Vilé, G.; Albani, D.; Nachtegaal, M.; Chen, Z.; Dontsova, D.; Antonietti, M.; López, N.; Pérez-Ramírez, J. A Stable Single-Site Palladium Catalyst for Hydrogenations. *Angew. Chem., Int. Ed.* **2015**, *54*, 11265−11269.
(53) Li, X.; Xi, S.; Sun, L.; Dou, S.; Huang, Z.; Su, T.; Wang, X. Isolated FeN_4 Sites for Efficient Electrocatalytic CO_2 Reduction. *Adv. Sci.* **2020**, *7*, 2001545.
(54) Cao, Y.; Chen, S.; Luo, Q.; Yan, H.; Lin, Y.; Liu, W.; Cao, L.; Lu, J.; Yang, J.; Yao, T.; Wei, S. Atomic-Level Insight into Optimizing the Hydrogen Evolution Pathway over a Co_1-N_4 Single-Site Photocatalyst. *Angew. Chem., Int. Ed.* **2017**, *56*, 12191−12196.
(55) Yan, H.; Cheng, H.; Yi, H.; Lin, Y.; Yao, T.; Wang, C.; Li, J.; Wei, S.; Lu, J. Single-Atom Pd_1/Graphene Catalyst Achieved by Atomic Layer Deposition: Remarkable Performance in Selective Hydrogenation of 1,3-Butadiene. *J. Am. Chem. Soc.* **2015**, *137*, 10484−10487.
(56) Qu, Y.; Chen, B.; Li, Z.; Duan, X.; Wang, L.; Lin, Y.; Yuan, T.; Zhou, F.; Hu, Y.; Yang, Z.; Zhao, C.; Wang, J.; Zhao, C.; Hu, Y.; Wu, G.; Zhang, Q.; Xu, Q.; Liu, B.; Gao, P.; You, R.; Huang, W.; Zheng, L.; Gu, L.; Wu, Y.; Li, Y. Thermal Emitting Strategy to Synthesize Atomically Dispersed Pt Metal Sites from Bulk Pt Metal. *J. Am. Chem. Soc.* **2019**, *141*, 4505−4509.
(57) Zhang, X.; Cui, G.; Feng, H.; Chen, L.; Wang, H.; Wang, B.; Zhang, X.; Zheng, L.; Hong, S.; Wei, M. Platinum-copper single atom alloy catalysts with high performance towards glycerol hydrogenolysis. *Nat. Commun.* **2019**, *10*, 5812.
(58) Ge, J.; He, D.; Chen, W.; Ju, H.; Zhang, H.; Chao, T.; Wang, X.; You, R.; Lin, Y.; Wang, Y.; Zhu, J.; Li, H.; Xiao, B.; Huang, W.; Wu, Y.; Hong, X.; Li, Y. Atomically Dispersed Ru on Ultrathin Pd Nanoribbons. *J. Am. Chem. Soc.* **2016**, *138*, 13850−13853.
(59) Chen, S.; Wang, B.; Zhu, J.; Wang, L.; Ou, H.; Zhang, Z.; Liang, X.; Zheng, L.; Zhou, L.; Su, Y.-Q.; Wang, D.; Li, Y. Lewis Acid Site-Promoted Single-Atomic Cu Catalyzes Electrochemical CO_2 Methanation. *Nano Lett.* **2021**, *21*, 7325−7331.
(60) Zhang, J.; Yin, R.; Shao, Q.; Zhu, T.; Huang, X. Oxygen Vacancies in Amorphous InO_x Nanoribbons Enhance CO_2 Adsorption and Activation for CO_2 Electroreduction. *Angew. Chem., Int. Ed.* **2019**, *58*, 5609−5613.
(61) Zhang, M.; Xu, W.; Ma, C.-L.; Yu, J.; Liu, Y.-T.; Ding, B. Highly Active and Selective Electroreduction of N_2 by the Catalysis of Ga Single Atoms Stabilized on Amorphous TiO_2 Nanofibers. *ACS Nano* **2022**, *16*, 4186−4196.
(62) Wang, Y.; Yan, D.; El Hankari, S.; Zou, Y.; Wang, S. Recent Progress on Layered Double Hydroxides and Their Derivatives for Electrocatalytic Water Splitting. *Adv. Sci.* **2018**, *5*, 1800064.
(63) Zhang, J.; Liu, J.; Xi, L.; Yu, Y.; Chen, N.; Sun, S.; Wang, W.; Lange, K. M.; Zhang, B. Single-Atom Au/NiFe Layered Double Hydroxide Electrocatalyst: Probing the Origin of Activity for Oxygen Evolution Reaction. *J. Am. Chem. Soc.* **2018**, *140*, 3876−3879.

https://doi.org/10.1021/acsnano.2c06827
ACS Nano 2022, 16, 17572−17592

(64) Kale, M. B.; Borse, R. A.; Gomaa Abdelkader Mohamed, A.; Wang, Y. Electrocatalysts by Electrodeposition: Recent Advances, Synthesis Methods, and Applications in Energy Conversion. *Adv. Funct. Mater.* **2021**, *31*, 2101313.
(65) Zhang, L.; Han, L.; Liu, H.; Liu, X.; Luo, J. Potential-Cycling Synthesis of Single Platinum Atoms for Efficient Hydrogen Evolution in Neutral Media. *Angew. Chem., Int. Ed.* **2017**, *56*, 13694−13698.
(66) Zhang, Z.; Feng, C.; Liu, C.; Zuo, M.; Qin, L.; Yan, X.; Xing, Y.; Li, H.; Si, R.; Zhou, S.; Zeng, J. Electrochemical deposition as a universal route for fabricating single-atom catalysts. *Nat. Commun.* **2020**, *11*, 1215.
(67) Stegelmann, C.; Andreasen, A.; Campbell, C. T. Degree of Rate Control: How Much the Energies of Intermediates and Transition States Control Rates. *J. Am. Chem. Soc.* **2009**, *131*, 8077−8082.
(68) Yang, X.; Wang, Y.; Tong, X.; Yang, N. Strain Engineering in Electrocatalysts: Fundamentals, Progress, and Perspectives. *Adv. Energy Mater.* **2022**, *12*, 2102261.
(69) Schlapka, A.; Lischka, M.; Groß, A.; Käsberger, U.; Jakob, P. Surface Strain versus Substrate Interaction in Heteroepitaxial Metal Layers: Pt on Ru(0001). *Phys. Rev. Lett.* **2003**, *91*, 016101.
(70) Bu, L.; Zhang, N.; Guo, S.; Zhang, X.; Li, J.; Yao, J.; Wu, T.; Lu, G.; Ma, J.-Y.; Su, D.; Huang, X. Biaxially strained PtPb/Pt core/shell nanoplate boosts oxygen reduction catalysis. *Science* **2016**, *354*, 1410−1414.
(71) Strasser, P.; Koh, S.; Anniyev, T.; Greeley, J.; More, K.; Yu, C.; Liu, Z.; Kaya, S.; Nordlund, D.; Ogasawara, H.; Toney, M. F.; Nilsson, A. Lattice-strain control of the activity in dealloyed core-shell fuel cell catalysts. *Nat. Chem.* **2010**, *2*, 454−460.
(72) He, J.; Shen, Y.; Yang, M.; Zhang, H.; Deng, Q.; Ding, Y. The effect of surface strain on the CO-poisoned surface of Pt electrode for hydrogen adsorption. *J. Catal.* **2017**, *350*, 212−217.
(73) Jiang, K.; Luo, M.; Liu, Z.; Peng, M.; Chen, D.; Lu, Y.-R.; Chan, T.-S.; de Groot, F. M. F.; Tan, Y. Rational strain engineering of single-atom ruthenium on nanoporous MoS_2 for highly efficient hydrogen evolution. *Nat. Commun.* **2021**, *12*, 1687.
(74) He, F.; Zhao, Y.; Yang, X.; Zheng, S.; Yang, B.; Li, Z.; Kuang, Y.; Zhang, Q.; Lei, L.; Qiu, M.; Dai, L.; Hou, Y. Metal−Organic Frameworks with Assembled Bifunctional Microreactor for Charge Modulation and Strain Generation toward Enhanced Oxygen Electrocatalysis. *ACS Nano* **2022**, *16*, 9523−9534.
(75) Zhou, X.; Jin, H.; Xia, B. Y.; Davey, K.; Zheng, Y.; Qiao, S.-Z. Molecular Cleavage of Metal-Organic Frameworks and Application to Energy Storage and Conversion. *Adv. Mater.* **2021**, *33*, 2104341.
(76) Luo, S.; Zhang, L.; Liao, Y.; Li, L.; Yang, Q.; Wu, X.; Wu, X.; He, D.; He, C.; Chen, W.; Wu, Q.; Li, M.; Hensen, E. J. M.; Quan, Z. A Tensile-Strained Pt−Rh Single-Atom Alloy Remarkably Boosts Ethanol Oxidation. *Adv. Mater.* **2021**, *33*, 2008508.
(77) Han, G.; Zhang, X.; Liu, W.; Zhang, Q.; Wang, Z.; Cheng, J.; Yao, T.; Gu, L.; Du, C.; Gao, Y.; Yin, G. Substrate strain tunes operando geometric distortion and oxygen reduction activity of CuN_2C_2 single-atom sites. *Nat. Commun.* **2021**, *12*, 6335.
(78) Haddon, R. C. Chemistry of the Fullerenes: The Manifestation of Strain in a Class of Continuous Aromatic Molecules. *Science* **1993**, *261*, 1545−1550.
(79) Xiao, M.; Gao, L.; Wang, Y.; Wang, X.; Zhu, J.; Jin, Z.; Liu, C.; Chen, H.; Li, G.; Ge, J.; He, Q.; Wu, Z.; Chen, Z.; Xing, W. Engineering Energy Level of Metal Center: Ru Single-Atom Site for Efficient and Durable Oxygen Reduction Catalysis. *J. Am. Chem. Soc.* **2019**, *141*, 19800−19806.
(80) Ramaswamy, N.; Tylus, U.; Jia, Q.; Mukerjee, S. Activity Descriptor Identification for Oxygen Reduction on Nonprecious Electrocatalysts: Linking Surface Science to Coordination Chemistry. *J. Am. Chem. Soc.* **2013**, *135*, 15443−15449.
(81) Yang, J.; Wang, Z.; Huang, C.-X.; Zhang, Y.; Zhang, Q.; Chen, C.; Du, J.; Zhou, X.; Zhang, Y.; Zhou, H.; Wang, L.; Zheng, X.; Gu, L.; Yang, L.-M.; Wu, Y. Compressive Strain Modulation of Single Iron Sites on Helical Carbon Support Boosts Electrocatalytic Oxygen Reduction. *Angew. Chem., Int. Ed.* **2021**, *60*, 22722−22728.
(82) Li, X.; Zhou, Q.; Wang, S.; Li, Y.; Liu, Y.; Gao, Q.; Wu, Q. Tuning the Coordination Environment to Effect the Electrocatalytic Behavior of a Single-Atom Catalyst toward the Nitrogen Reduction Reaction. *J. Phys. Chem. C* **2021**, *125*, 11963−11974.
(83) Spöri, C.; Kwan, J. T. H.; Bonakdarpour, A.; Wilkinson, D. P.; Strasser, P. The Stability Challenges of Oxygen Evolving Catalysts: Towards a Common Fundamental Understanding and Mitigation of Catalyst Degradation. *Angew. Chem., Int. Ed.* **2017**, *56*, 5994−6021.
(84) Fabbri, E.; Habereder, A.; Waltar, K.; Kötz, R.; Schmidt, T. J. Developments and perspectives of oxide-based catalysts for the oxygen evolution reaction. *Catal. Sci. Technol.* **2014**, *4*, 3800−3821.
(85) Yao, Y.; Hu, S.; Chen, W.; Huang, Z.-Q.; Wei, W.; Yao, T.; Liu, R.; Zang, K.; Wang, X.; Wu, G.; Yuan, W.; Yuan, T.; Zhu, B.; Liu, W.; Li, Z.; He, D.; Xue, Z.; Wang, Y.; Zheng, X.; Dong, J.; Chang, C.-R.; Chen, Y.; Hong, X.; Luo, J.; Wei, S.; Li, W.-X.; Strasser, P.; Wu, Y.; Li, Y. Engineering the electronic structure of single atom Ru sites via compressive strain boosts acidic water oxidation electrocatalysis. *Nat. Catal.* **2019**, *2*, 304−313.
(86) Denton, A. R.; Ashcroft, N. W. Vegard's law. *Phys. Rev. A* **1991**, *43*, 3161−3164.
(87) Medford, A. J.; Vojvodic, A.; Hummelshøj, J. S.; Voss, J.; Abild-Pedersen, F.; Studt, F.; Bligaard, T.; Nilsson, A.; Nørskov, J. K. From the Sabatier principle to a predictive theory of transition-metal heterogeneous catalysis. *J. Catal.* **2015**, *328*, 36−42.
(88) Li, Z.; Zhuang, Z.; Lv, F.; Zhu, H.; Zhou, L.; Luo, M.; Zhu, J.; Lang, Z.; Feng, S.; Chen, W.; Mai, L.; Guo, S. The Marriage of the FeN_4 Moiety and MXene Boosts Oxygen Reduction Catalysis: Fe 3d Electron Delocalization Matters. *Adv. Mater.* **2018**, *30*, 1803220.
(89) Shen, G.; Zhang, R.; Pan, L.; Hou, F.; Zhao, Y.; Shen, Z.; Mi, W.; Shi, C.; Wang, Q.; Zhang, X.; Zou, J.-J. Regulating the Spin State of FeIII by Atomically Anchoring on Ultrathin Titanium Dioxide for Efficient Oxygen Evolution Electrocatalysis. *Angew. Chem., Int. Ed.* **2020**, *59*, 2313−2317.
(90) Liu, Y.; Liu, X.; Lv, Z.; Liu, R.; Li, L.; Wang, J.; Yang, W.; Jiang, X.; Feng, X.; Wang, B. Tuning the Spin State of the Iron Center by Bridge-Bonded Fe-O-Ti Ligands for Enhanced Oxygen Reduction. *Angew. Chem., Int. Ed.* **2022**, *61*, e202117617.
(91) Sun, S.; Sun, Y.; Zhou, Y.; Xi, S.; Ren, X.; Huang, B.; Liao, H.; Wang, L. P.; Du, Y.; Xu, Z. J. Shifting Oxygen Charge Towards Octahedral Metal: A Way to Promote Water Oxidation on Cobalt Spinel Oxides. *Angew. Chem., Int. Ed.* **2019**, *58*, 6042−6047.
(92) Sun, Y.; Ren, X.; Sun, S.; Liu, Z.; Xi, S.; Xu, Z. J. Engineering High-Spin State Cobalt Cations in Spinel Zinc Cobalt Oxide for Spin Channel Propagation and Active Site Enhancement in Water Oxidation. *Angew. Chem., Int. Ed.* **2021**, *60*, 14536−14544.
(93) Dal Santo, V.; Guidotti, M.; Psaro, R.; Marchese, L.; Carniato, F.; Bisio, C. Rational design of single-site heterogeneous catalysts: towards high chemo-, regio- and stereoselectivity. *Proc. R. Soc. A: Math. Phys. Eng. Sci.* **2012**, *468*, 1904−1926.
(94) Liu, Y.; McCrory, C. C. L. Modulating the mechanism of electrocatalytic CO_2 reduction by cobalt phthalocyanine through polymer coordination and encapsulation. *Nat. Commun.* **2019**, *10*, 1683.
(95) Bhugun, I.; Anson, F. C. Enhancement of the Catalytic Activity of a Macrocyclic Cobalt(II) Complex for the Electroreduction of O_2 by Adsorption on Graphite. *Inorg. Chem.* **1996**, *35*, 7253−7259.
(96) Wang, J.; Huang, X.; Xi, S.; Lee, J.-M.; Wang, C.; Du, Y.; Wang, X. Linkage Effect in the Heterogenization of Cobalt Complexes by Doped Graphene for Electrocatalytic CO_2 Reduction. *Angew. Chem., Int. Ed.* **2019**, *58*, 13532−13539.
(97) Kramer, W. W.; McCrory, C. C. L. Polymer coordination promotes selective CO_2 reduction by cobalt phthalocyanine. *Chem. Sci.* **2016**, *7*, 2506−2515.
(98) Laviron, E. The use of linear potential sweep voltammetry and of a.c. voltammetry for the study of the surface electrochemical reaction of strongly adsorbed systems and of redox modified electrodes. *J. electroanal. chem. interfacial electrochem.* **1979**, *100*, 263−270.
(99) McQueen, E. W.; Goldsmith, J. I. Electrochemical Analysis of Single-Walled Carbon Nanotubes Functionalized with Pyrene-Pendant

Transition Metal Complexes. *J. Am. Chem. Soc.* **2009**, *131*, 17554−17556.
(100) Hunter, C. A.; Sanders, J. K. M. The nature of. pi.-pi. interactions. *J. Am. Chem. Soc.* **1990**, *112*, 5525−5534.
(101) Pan, Y.; Lin, R.; Chen, Y.; Liu, S.; Zhu, W.; Cao, X.; Chen, W.; Wu, K.; Cheong, W.-C.; Wang, Y.; Zheng, L.; Luo, J.; Lin, Y.; Liu, Y.; Liu, C.; Li, J.; Lu, Q.; Chen, X.; Wang, D.; Peng, Q.; Chen, C.; Li, Y. Design of Single-Atom Co-N_5 Catalytic Site: A Robust Electrocatalyst for CO2 Reduction with Nearly 100% CO Selectivity and Remarkable Stability. *J. Am. Chem. Soc.* **2018**, *140*, 4218−4221.
(102) Sun, L.; Reddu, V.; Su, T.; Chen, X.; Wu, T.; Dai, W.; Fisher, A. C.; Wang, X. Effects of Axial Functional Groups on Heterogeneous Molecular Catalysts for Electrocatalytic CO_2 Reduction. *Small Structures* **2021**, *2*, 2100093.
(103) Liu, X.; Liu, Y.; Yang, W.; Feng, X.; Wang, B. Controlled Modification of Axial Coordination for Transition-Metal Single-Atom Electrocatalyst. *Chem.—Eur. J.* **2022**, *28*, e202201471.
(104) Zhang, H.; Li, J.; Xi, S.; Du, Y.; Hai, X.; Wang, J.; Xu, H.; Wu, G.; Zhang, J.; Lu, J.; Wang, J. A Graphene-Supported Single-Atom FeN_5 Catalytic Site for Efficient Electrochemical CO_2 Reduction. *Angew. Chem., Int. Ed.* **2019**, *58*, 14871−14876.
(105) Geng, Z.; Kong, X.; Chen, W.; Su, H.; Liu, Y.; Cai, F.; Wang, G.; Zeng, J. Oxygen Vacancies in ZnO Nanosheets Enhance CO_2 Electrochemical Reduction to CO. *Angew. Chem., Int. Ed.* **2018**, *57*, 6054−6059.
(106) Kozachuk, O.; Luz, I.; Llabrés i Xamena, F. X.; Noei, H.; Kauer, M.; Albada, H. B.; Bloch, E. D.; Marler, B.; Wang, Y.; Muhler, M.; Fischer, R. A. Multifunctional, Defect-Engineered Metal-Organic Frameworks with Ruthenium Centers: Sorption and Catalytic Properties. *Angew. Chem., Int. Ed.* **2014**, *53*, 7058−7062.
(107) Liu, S.; Yang, H. B.; Hung, S.-F.; Ding, J.; Cai, W.; Liu, L.; Gao, J.; Li, X.; Ren, X.; Kuang, Z.; Huang, Y.; Zhang, T.; Liu, B. Inside Cover: Elucidating the Electrocatalytic CO_2 Reduction Reaction over a Model Single-Atom Nickel Catalyst. *Angew. Chem., Int. Ed.* **2020**, *59*, 510−510.
(108) Chen, K.; Cao, M.; Lin, Y.; Fu, J.; Liao, H.; Zhou, Y.; Li, H.; Qiu, X.; Hu, J.; Zheng, X.; Shakouri, M.; Xiao, Q.; Hu, Y.; Li, J.; Liu, J.; Cortés, E.; Liu, M. Ligand Engineering in Nickel Phthalocyanine to Boost the Electrocatalytic Reduction of CO_2. *Adv. Funct. Mater.* **2022**, *32*, 2111322.
(109) Kim, H.; Shin, D.; Yang, W.; Won, D. H.; Oh, H.-S.; Chung, M. W.; Jeong, D.; Kim, S. H.; Chae, K. H.; Ryu, J. Y.; Lee, J.; Cho, S. J.; Seo, J.; Kim, H.; Choi, C. H. Identification of Single-Atom Ni Site Active toward Electrochemical CO_2 Conversion to CO. *J. Am. Chem. Soc.* **2021**, *143*, 925−933.
(110) Zhang, X.; Wang, Y.; Gu, M.; Wang, M.; Zhang, Z.; Pan, W.; Jiang, Z.; Zheng, H.; Lucero, M.; Wang, H.; Sterbinsky, G. E.; Ma, Q.; Wang, Y.-G.; Feng, Z.; Li, J.; Dai, H.; Liang, Y. Molecular engineering of dispersed nickel phthalocyanines on carbon nanotubes for selective CO_2 reduction. *Nat. Energy.* **2020**, *5*, 684−692.
(111) Wu, Y.; Jiang, Z.; Lu, X.; Liang, Y.; Wang, H. Domino electroreduction of CO_2 to methanol on a molecular catalyst. *Nature* **2019**, *575*, 639−642.
(112) Li, R.; Zhang, X.; Zhu, P.; Ng, D. K. P.; Kobayashi, N.; Jiang, J. Electron-Donating or -Withdrawing Nature of Substituents Revealed by the Electrochemistry of Metal-Free Phthalocyanines. *Inorg. Chem.* **2006**, *45*, 2327−2334.
(113) Jia, Q.; Ramaswamy, N.; Hafiz, H.; Tylus, U.; Strickland, K.; Wu, G.; Barbiellini, B.; Bansil, A.; Holby, E. F.; Zelenay, P.; Mukerjee, S. Experimental Observation of Redox-Induced Fe-N Switching Behavior as a Determinant Role for Oxygen Reduction Activity. *ACS Nano* **2015**, *9*, 12496−12505.
(114) Kwon, N. H.; Kim, M.; Jin, X.; Lim, J.; Kim, I. Y.; Lee, N.-S.; Kim, H.; Hwang, S.-J. A rational method to kinetically control the rate-determining step to explore efficient electrocatalysts for the oxygen evolution reaction. *NPG Asia Mater.* **2018**, *10*, 659−669.
(115) Costentin, C.; Savéant, J.-M. Towards an intelligent design of molecular electrocatalysts. *Nat. Rev. Chem.* **2017**, *1*, 0087.
(116) Kim, N.-I.; Sa, Y. J.; Yoo, T. S.; Choi, S. R.; Afzal, R. A.; Choi, T.; Seo, Y.-S.; Lee, K.-S.; Hwang, J. Y.; Choi, W. S.; Joo, S. H.; Park, J.-Y. Oxygen-deficient triple perovskites as highly active and durable bifunctional electrocatalysts for oxygen electrode reactions. *Sci. Adv.* **2018**, *4*, eaap9360.
(117) Liu, W.; Zheng, D.; Deng, T.; Chen, Q.; Zhu, C.; Pei, C.; Li, H.; Wu, F.; Shi, W.; Yang, S.-W.; Zhu, Y.; Cao, X. Boosting Electrocatalytic Activity of 3d-Block Metal (Hydro)oxides by Ligand-Induced Conversion. *Angew. Chem., Int. Ed.* **2021**, *60*, 10614−10619.
(118) Yarlagadda, V.; Carpenter, M. K.; Moylan, T. E.; Kukreja, R. S.; Koestner, R.; Gu, W.; Thompson, L.; Kongkanand, A. Boosting Fuel Cell Performance with Accessible Carbon Mesopores. *ACS Energy Lett.* **2018**, *3*, 618−621.
(119) Wu, Z.-Y.; Zhu, P.; Cullen, D. A.; Hu, Y.; Yan, Q.-Q.; Shen, S.-C.; Chen, F.-Y.; Yu, H.; Shakouri, M.; Arregui-Mena, J. D.; Ziabari, A.; Paterson, A. R.; Liang, H.-W.; Wang, H. A general synthesis of single atom catalysts with controllable atomic and mesoporous structures. *Nat. Synth.* **2022**, *1*, 658−667.
(120) Marken, F.; Neudeck, A.; Bond, A. M. Cyclic Voltammetry. In *Electroanalytical Methods: Guide to Experiments and Applications*; Scholz, F., Bond, A. M., Compton, R. G., Fiedler, D. A., Inzelt, G., Kahlert, H., Komorsky-Lovrić, Š., Lohse, H., Lovrić, M., Marken, F., Neudeck, A., Retter, U., Scholz, F., Stojek, Z., Eds.; Springer Berlin Heidelberg: Berlin, Heidelberg, 2010; pp 57−106, DOI: 10.1007/978-3-642-02915-8_4.
(121) Wu, Z.-Y.; Xu, S.-L.; Yan, Q.-Q.; Chen, Z.-Q.; Ding, Y.-W.; Li, C.; Liang, H.-W.; Yu, S.-H. Transition metal-assisted carbonization of small organic molecules toward functional carbon materials. *Sci. Adv.* **2018**, *4*, eaat0788.
(122) Cheng, N.; Ren, L.; Xu, X.; Du, Y.; Dou, S. X. Recent Development of Zeolitic Imidazolate Frameworks (ZIFs) Derived Porous Carbon Based Materials as Electrocatalysts. *Adv. Energy Mater.* **2018**, *8*, 1801257.
(123) Sun, G.; Wang, J.; Liu, X.; Long, D.; Qiao, W.; Ling, L. Ion Transport Behavior in Triblock Copolymer-Templated Ordered Mesoporous Carbons with Different Pore Symmetries. *J. Phys. Chem.* **2010**, *114*, 18745−18751.
(124) Lee, S. H.; Kim, J.; Chung, D. Y.; Yoo, J. M.; Lee, H. S.; Kim, M. J.; Mun, B. S.; Kwon, S. G.; Sung, Y.-E.; Hyeon, T. Design Principle of Fe-N-C Electrocatalysts: How to Optimize Multimodal Porous Structures? *J. Am. Chem. Soc.* **2019**, *141*, 2035−2045.
(125) Lee, J. H.; Lee, H. J.; Lim, S. Y.; Kim, B. G.; Choi, J. W. Combined CO_2-philicity and Ordered Mesoporosity for Highly Selective CO_2 Capture at High Temperatures. *J. Am. Chem. Soc.* **2015**, *137*, 7210−7216.
(126) Wan, Y.; Zhao. On the Controllable Soft-Templating Approach to Mesoporous Silicates. *Chem. Rev.* **2007**, *107*, 2821−2860.
(127) Kim, J. M.; Sakamoto, Y.; Hwang, Y. K.; Kwon, Y.-U.; Terasaki, O.; Park, S.-E.; Stucky, G. D. Structural Design of Mesoporous Silica by Micelle-Packing Control Using Blends of Amphiphilic Block Copolymers. *J. Phys. Chem. B* **2002**, *106*, 2552−2558.
(128) Han, X.; Zhang, T.; Wang, X.; Zhang, Z.; Li, Y.; Qin, Y.; Wang, B.; Han, A.; Liu, J. Hollow mesoporous atomically dispersed metal-nitrogen-carbon catalysts with enhanced diffusion for catalysis involving larger molecules. *Nat. Commun.* **2022**, *13*, 2900.
(129) Feng, L.; Yuan, S.; Zhang, L.-L.; Tan, K.; Li, J.-L.; Kirchon, A.; Liu, L.-M.; Zhang, P.; Han, Y.; Chabal, Y. J.; Zhou, H.-C. Creating Hierarchical Pores by Controlled Linker Thermolysis in Multivariate Metal−Organic Frameworks. *J. Am. Chem. Soc.* **2018**, *140*, 2363−2372.
(130) Naghdi, S.; Cherevan, A.; Giesriegl, A.; Guillet-Nicolas, R.; Biswas, S.; Gupta, T.; Wang, J.; Haunold, T.; Bayer, B. C.; Rupprechter, G.; Toroker, M. C.; Kleitz, F.; Eder, D. Selective ligand removal to improve accessibility of active sites in hierarchical MOFs for heterogeneous photocatalysis. *Nat. Commun.* **2022**, *13*, 282.
(131) Ye, L.; Chai, G.; Wen, Z. Zn-MOF-74 Derived N-Doped Mesoporous Carbon as pH-Universal Electrocatalyst for Oxygen Reduction Reaction. *Adv. Funct. Mater.* **2017**, *27*, 1606190.
(132) Ye, L.; Ying, Y.; Sun, D.; Zhang, Z.; Fei, L.; Wen, Z.; Qiao, J.; Huang, H. Highly Efficient Porous Carbon Electrocatalyst with Controllable N-Species Content for Selective CO_2 Reduction. *Angew. Chem., Int. Ed.* **2020**, *59*, 3244−3251.

(133) Feng, Q.; Zhao, S.; Xu, Q.; Chen, W.; Tian, S.; Wang, Y.; Yan, W.; Luo, J.; Wang, D.; Li, Y. Mesoporous Nitrogen-Doped Carbon-Nanosphere-Supported Isolated Single-Atom Pd Catalyst for Highly Efficient Semihydrogenation of Acetylene. *Adv. Mater.* **2019**, *31*, 1901024.
(134) Liang, H.-W.; Zhuang, X.; Brüller, S.; Feng, X.; Müllen, K. Hierarchically porous carbons with optimized nitrogen doping as highly active electrocatalysts for oxygen reduction. *Nat. Commun.* **2014**, *5*, 4973.
(135) Zhang, H.; Noonan, O.; Huang, X.; Yang, Y.; Xu, C.; Zhou, L.; Yu, C. Surfactant-Free Assembly of Mesoporous Carbon Hollow Spheres with Large Tunable Pore Sizes. *ACS Nano* **2016**, *10*, 4579−4586.
(136) Qiao, Z.-A.; Guo, B.; Binder, A. J.; Chen, J.; Veith, G. M.; Dai, S. Controlled Synthesis of Mesoporous Carbon Nanostructures via a "Silica-Assisted" Strategy. *Nano Lett.* **2013**, *13*, 207−212.
(137) Liu, L.; Corma, A. Metal Catalysts for Heterogeneous Catalysis: From Single Atoms to Nanoclusters and Nanoparticles. *Chem. Rev.* **2018**, *118*, 4981−5079.
(138) Li, H.; Wang, L.; Dai, Y.; Pu, Z.; Lao, Z.; Chen, Y.; Wang, M.; Zheng, X.; Zhu, J.; Zhang, W.; Si, R.; Ma, C.; Zeng, J. Synergetic interaction between neighbouring platinum monomers in CO_2 hydrogenation. *Nat. Nanotechnol.* **2018**, *13*, 411−417.
(139) Geng, S.-K.; Zheng, Y.; Li, S.-Q.; Su, H.; Zhao, X.; Hu, J.; Shu, H.-B.; Jaroniec, M.; Chen, P.; Liu, Q.-H.; Qiao, S.-Z. Nickel ferrocyanide as a high-performance urea oxidation electrocatalyst. *Nat. Energy.* **2021**, *6*, 904−912.
(140) Shan, J.; Ye, C.; Jiang, Y.; Jaroniec, M.; Zheng, Y.; Qiao, S.-Z. Metal-metal interactions in correlated single-atom catalysts. *Sci. Adv.* **2022**, *8*, eabo0762.
(141) Shan, J.; Ye, C.; Chen, S.; Sun, T.; Jiao, Y.; Liu, L.; Zhu, C.; Song, L.; Han, Y.; Jaroniec, M.; Zhu, Y.; Zheng, Y.; Qiao, S.-Z. Short-Range Ordered Iridium Single Atoms Integrated into Cobalt Oxide Spinel Structure for Highly Efficient Electrocatalytic Water Oxidation. *J. Am. Chem. Soc.* **2021**, *143*, 5201−5211.
(142) Chen, H.; Wu, Q.; Wang, Y.; Zhao, Q.; Ai, X.; Shen, Y.; Zou, X. d−sp orbital hybridization: a strategy for activity improvement of transition metal catalysts. *Chem. Commun.* **2022**, *58*, 7730−7740.
(143) Du, X.; Huang, J.; Zhang, J.; Yan, Y.; Wu, C.; Hu, Y.; Yan, C.; Lei, T.; Chen, W.; Fan, C.; Xiong, J. Modulating Electronic Structures of Inorganic Nanomaterials for Efficient Electrocatalytic Water Splitting. *Angew. Chem., Int. Ed.* **2019**, *58*, 4484−4502.
(144) Jin, Z.; Li, P.; Meng, Y.; Fang, Z.; Xiao, D.; Yu, G. Understanding the inter-site distance effect in single-atom catalysts for oxygen electroreduction. *Nat. Catal.* **2021**, *4*, 615−622.
(145) Cao, L.; Shao, Y.; Pan, H.; Lu, Z. Designing Efficient Dual-Metal Single-Atom Electrocatalyst $TMZnN_6$ (TM = Mn, Fe, Co, Ni, Cu, Zn) for Oxygen Reduction Reaction. *J. Phys. Chem. C* **2020**, *124*, 11301−11307.
(146) Wang, S.; Shi, L.; Bai, X.; Li, Q.; Ling, C.; Wang, J. Highly Efficient Photo-/Electrocatalytic Reduction of Nitrogen into Ammonia by Dual-Metal Sites. *ACS Cent. Sci.* **2020**, *6*, 1762−1771.
(147) Ying, Y.; Luo, X.; Qiao, J.; Huang, H. More is Different:" Synergistic Effect and Structural Engineering in Double-Atom Catalysts. *Adv. Funct. Mater.* **2021**, *31*, 2007423.
(148) Hou, C.-C.; Wang, H.-F.; Li, C.; Xu, Q. From metal-organic frameworks to single/dual-atom and cluster metal catalysts for energy applications. *Energy Environ. Sci.* **2020**, *13*, 1658−1693.
(149) Chen, C.; Sun, M.; Wang, K.; Li, Y. Dual-metal single-atomic catalyst: The challenge in synthesis, characterization, and mechanistic investigation for electrocatalysis. *SmartMat* **2022**, DOI: 10.1002/smm2.1085.
(150) Zhang, D.; Chen, W.; Li, Z.; Chen, Y.; Zheng, L.; Gong, Y.; Li, Q.; Shen, R.; Han, Y.; Cheong, W.-C.; Gu, L.; Li, Y. Isolated Fe and Co dual active sites on nitrogen-doped carbon for a highly efficient oxygen reduction reaction. *Chem. Commun.* **2018**, *54*, 4274−4277.
(151) Zhao, R.; Liang, Z.; Gao, S.; Yang, C.; Zhu, B.; Zhao, J.; Qu, C.; Zou, R.; Xu, Q. Puffing Up Energetic Metal-Organic Frameworks to Large Carbon Networks with Hierarchical Porosity and Atomically Dispersed Metal Sites. *Angew. Chem., Int. Ed.* **2019**, *58*, 1975−1979.
(152) Fang, X.; Jiao, L.; Yu, S.-H.; Jiang, H.-L. Metal-Organic Framework-Derived FeCo-N-Doped Hollow Porous Carbon Nanocubes for Electrocatalysis in Acidic and Alkaline Media. *ChemSusChem* **2017**, *10*, 3019−3024.
(153) Sarkar, S.; Biswas, A.; Siddharthan, E. E.; Thapa, R.; Dey, R. S. Strategic Modulation of Target-Specific Isolated Fe,Co Single-Atom Active Sites for Oxygen Electrocatalysis Impacting High Power Zn−Air Battery. *ACS Nano* **2022**, *16*, 7890−7903.
(154) Zhu, Z.; Yin, H.; Wang, Y.; Chuang, C.-H.; Xing, L.; Dong, M.; Lu, Y.-R.; Casillas-Garcia, G.; Zheng, Y.; Chen, S.; Dou, Y.; Liu, P.; Cheng, Q.; Zhao, H. Coexisting Single-Atomic Fe and Ni Sites on Hierarchically Ordered Porous Carbon as a Highly Efficient ORR Electrocatalyst. *Adv. Mater.* **2020**, *32*, 2004670.
(155) Shen, K.; Zhang, L.; Chen, X.; Liu, L.; Zhang, D.; Han, Y.; Chen, J.; Long, J.; Luque, R.; Li, Y.; Chen, B. Ordered macro-microporous metal-organic framework single crystals. *Science* **2018**, *359*, 206−210.
(156) Lin, L.; Li, H.; Yan, C.; Li, H.; Si, R.; Li, M.; Xiao, J.; Wang, G.; Bao, X. Synergistic Catalysis over Iron-Nitrogen Sites Anchored with Cobalt Phthalocyanine for Efficient CO_2 Electroreduction. *Adv. Mater.* **2019**, *31*, 1903470.
(157) Chen, J.; Li, H.; Fan, C.; Meng, Q.; Tang, Y.; Qiu, X.; Fu, G.; Ma, T. Dual Single-Atomic Ni-N_4 and Fe-N_4 Sites Constructing Janus Hollow Graphene for Selective Oxygen Electrocatalysis. *Adv. Mater.* **2020**, *32*, 2003134.
(158) Sa, Y. J.; Joo, S. H. Dimeric Fe Sites Effectively Activate Oxygen Molecule. *Chem.* **2019**, *5*, 3006−3007.
(159) Puglia, C.; Nilsson, A.; Hernnäs, B.; Karis, O.; Bennich, P.; Mårtensson, N. Physisorbed, chemisorbed and dissociated O_2 on Pt(111) studied by different core level spectroscopy methods. *Surf. Sci.* **1995**, *342*, 119−133.
(160) Wang, Y.; Park, B. J.; Paidi, V. K.; Huang, R.; Lee, Y.; Noh, K.-J.; Lee, K.-S.; Han, J. W. Precisely Constructing Orbital Coupling-Modulated Dual-Atom Fe Pair Sites for Synergistic CO_2 Electroreduction. *ACS Energy Lett.* **2022**, *7*, 640−649.
(161) Fonseca, J.; Lu, J. Single-Atom Catalysts Designed and Prepared by the Atomic Layer Deposition Technique. *ACS Catal.* **2021**, *11*, 7018−7059.
(162) Yan, H.; Lin, Y.; Wu, H.; Zhang, W.; Sun, Z.; Cheng, H.; Liu, W.; Wang, C.; Li, J.; Huang, X.; Yao, T.; Yang, J.; Wei, S.; Lu, J. Bottom-up precise synthesis of stable platinum dimers on graphene. *Nat. Commun.* **2017**, *8*, 1070.
(163) Jiao, J.; Lin, R.; Liu, S.; Cheong, W.-C.; Zhang, C.; Chen, Z.; Pan, Y.; Tang, J.; Wu, K.; Hung, S.-F.; Chen, H. M.; Zheng, L.; Lu, Q.; Yang, X.; Xu, B.; Xiao, H.; Li, J.; Wang, D.; Peng, Q.; Chen, C.; Li, Y. Copper atom-pair catalyst anchored on alloy nanowires for selective and efficient electrochemical reduction of CO_2. *Nat. Chem.* **2019**, *11*, 222−228.
(164) Li, S.; Guan, A.; Yang, C.; Peng, C.; Lv, X.; Ji, Y.; Quan, Y.; Wang, Q.; Zhang, L.; Zheng, G. Dual-Atomic Cu Sites for Electrocatalytic CO Reduction to C_{2+} Products. *ACS Mater. Lett.* **2021**, *3*, 1729−1737.
(165) Pedersen, A.; Barrio, J.; Li, A.; Jervis, R.; Brett, D. J. L.; Titirici, M. M.; Stephens, I. E. L. Dual-Metal Atom Electrocatalysts: Theory, Synthesis, Characterization, and Applications. *Adv. Energy Mater.* **2022**, *12*, 2102715.
(166) Liu, M.; Li, N.; Cao, S.; Wang, X.; Lu, X.; Kong, L.; Xu, Y.; Bu, X.-H. A "Pre-Constrained Metal Twins" Strategy to Prepare Efficient Dual-Metal-Atom Catalysts for Cooperative Oxygen Electrocatalysis. *Adv. Mater.* **2022**, *34*, 2107421.
(167) Cui, T.; Wang, Y.-P.; Ye, T.; Wu, J.; Chen, Z.; Li, J.; Lei, Y.; Wang, D.; Li, Y. Engineering Dual Single-Atom Sites on 2D Ultrathin N-doped Carbon Nanosheets Attaining Ultra-Low-Temperature Zinc-Air Battery. *Angew. Chem., Int. Ed.* **2022**, *61*, e202115219.
(168) Liu, X.; Giordano, C.; Antonietti, M. A Facile Molten-Salt Route to Graphene Synthesis. *Small* **2014**, *10*, 193−200.

(169) Fechler, N.; Fellinger, T.-P.; Antonietti, M. Salt Templating": A Simple and Sustainable Pathway toward Highly Porous Functional Carbons from Ionic Liquids. *Adv. Mater.* **2013**, *25*, 75−79.
(170) Liu, M.; Chun, H.; Yang, T.-C.; Hong, S. J.; Yang, C.-M.; Han, B.; Lee, L. Y. S. Tuning the Site-to-Site Interaction in Ru−M (M = Co, Fe, Ni) Diatomic Electrocatalysts to Climb up the Volcano Plot of Oxygen Electroreduction. *ACS Nano* **2022**, *16*, 10657−10666.
(171) Zhang, L.; Si, R.; Liu, H.; Chen, N.; Wang, Q.; Adair, K.; Wang, Z.; Chen, J.; Song, Z.; Li, J.; Banis, M. N.; Li, R.; Sham, T.-K.; Gu, M.; Liu, L.-M.; Botton, G. A.; Sun, X. Atomic layer deposited Pt-Ru dual-metal dimers and identifying their active sites for hydrogen evolution reaction. *Nat. Commun.* **2019**, *10*, 4936.
(172) Wang, J.; Gan, L.; Zhang, W.; Peng, Y.; Yu, H.; Yan, Q.; Xia, X.; Wang, X. In situ formation of molecular Ni-Fe active sites on heteroatom-doped graphene as a heterogeneous electrocatalyst toward oxygen evolution. *Sci. Adv.* **2018**, *4*, eaap7970.
(173) Canaguier, S.; Artero, V.; Fontecave, M. Modelling NiFe hydrogenases: nickel-based electrocatalysts for hydrogen production. *Dalton Trans.* **2008**, 315−325.
(174) Bai, L.; Hsu, C.-S.; Alexander, D. T. L.; Chen, H. M.; Hu, X. A Cobalt-Iron Double-Atom Catalyst for the Oxygen Evolution Reaction. *J. Am. Chem. Soc.* **2019**, *141*, 14190−14199.
(175) Zhou, X.; Gao, J.; Hu, Y.; Jin, Z.; Hu, K.; Reddy, K. M.; Yuan, Q.; Lin, X.; Qiu, H.-J. Theoretically Revealed and Experimentally Demonstrated Synergistic Electronic Interaction of CoFe Dual-Metal Sites on N-doped Carbon for Boosting Both Oxygen Reduction and Evolution Reactions. *Nano Lett.* **2022**, *22*, 3392−3399.
(176) Tong, Y.; Chen, P.; Zhang, M.; Zhou, T.; Zhang, L.; Chu, W.; Wu, C.; Xie, Y. Oxygen Vacancies Confined in Nickel Molybdenum Oxide Porous Nanosheets for Promoted Electrocatalytic Urea Oxidation. *ACS Catal.* **2018**, *8*, 1−7.
(177) Hunter, M. A.; Fischer, J. M. T. A.; Yuan, Q.; Hankel, M.; Searles, D. J. Evaluating the Catalytic Efficiency of Paired, Single-Atom Catalysts for the Oxygen Reduction Reaction. *ACS Catal.* **2019**, *9*, 7660−7667.
(178) Zhang, L.; Fischer, J. M. T. A.; Jia, Y.; Yan, X.; Xu, W.; Wang, X.; Chen, J.; Yang, D.; Liu, H.; Zhuang, L.; Hankel, M.; Searles, D. J.; Huang, K.; Feng, S.; Brown, C. L.; Yao, X. Coordination of Atomic Co-Pt Coupling Species at Carbon Defects as Active Sites for Oxygen Reduction Reaction. *J. Am. Chem. Soc.* **2018**, *140*, 10757−10763.

https://doi.org/10.1021/acsnano.2c06827
ACS Nano 2022, 16, 17572−17592